KAUNAS UNIVERSITY OF TECHNOLOGY
FACULTY OF MATHEMATICS AND NATURAL SCIENCES

Aleksandras Ševčik

MONTE CARLO MODELLING OF BRACHYTHERAPY SOURCE IN AN ANTHROPOMORPHIC HEAD PHANTOM

Final Master Degree Project

Supervisor:

Prof. Diana Adlienė (KTU)

KAUNAS, 2017

KAUNAS UNIVERSITY OF TECHNOLOGY
FACULTY OF MATHEMATICS AND NATURAL SCIENCES

MONTE CARLO MODELLING OF BRACHYTHERAPY SOURCE IN AN ANTHROPOMORPHIC HEAD PHANTOM

Final Master Degree Project
Medical Physics (code 621B92002)

Supervisor(s)
(signature) Prof. Diana Adlienė
(date)

Reviewer
(signature) Dr. Marius Kaminskas
(date)

Project prepared by
(signature) Aleksandras Ševčik
(date)

KAUNAS, 2017

KAUNAS UNIVERSITY OF TECHNOLOGY

(Faculty)

(Student's name, surname)

(Title and code of study programme)

"Title of Final Project"

DECLARATION OF ACADEMIC INTEGRITY

___ _____ 20 ____

Kaunas

I confirm that the final project of mine, **Aleksandras Ševčik**, on the subject *Monte Carlo modelling of brachytherapy source in an anthropomorphic head phantom* is written completely by myself; all the provided data and research results are correct and have been obtained honestly. None of the parts of this thesis have been plagiarized from any printed, Internet-based or otherwise recorded sources. All direct and indirect quotations from external resources are indicated in the list of references. No monetary funds (unless required by law) have been paid to anyone for any contribution to this thesis.

I fully and completely understand that any discovery of any manifestations/case/facts of dishonesty inevitably results in me incurring a penalty according to the procedure(s) effective at Kaunas University of Technology.

_____ _____

(name and surname filled in by hand) *(signature)*

TABLE OF CONTENTS

ABBREVIATIONS

2D	Two Dimensional
3D	Three Dimensional
AAPM	American Association of Physicists in Medicine
BREP	Boundary Representation (phantoms)
CCS	Collapsed Cone Superposition
CH	Condense History
CLT	Central Limit Theorem
CT	Computed Tomography
DICOM	Digital Imaging and Communications in Medicine
DVH	Dose Volume Histogram
GPU	Graphical Processor Unit
GUI	Graphical User Interface
HDR	High Dose Rate
HPCC	High Performance Computing Center
ICRU	International Commission on Radiation Units and Measurements
ICRP	International Commission on Radiological Protection
ICWG	Interstitial Collaborative Working Group
ISA	Inter-Seed Attenuation
LDR	Low Dose Rate
MBCDA	Model Based Dosimetry Calculation Algorithm
MC	Monte Carlo
MOSFET	Metal–Oxide–Semiconductor Field-Effect Transistor
MRI	Magnetic Resonance Imaging
NCPTS	National Center of Physical and Technology Sciences
PDF	Probability Distribution Function
QA	Quality Assurance
QMS	Quality Management Systems
SPD	Solid Polymeric Dosimeter
TLD	Thermoluminescence Dosimetry
TPS	Treatment Planning System

Ševčik, Aleksandras. Monte Carlo modelling of brachytherapy source in an anthropomorphic head phantom. Final Master Degree Project / supervisor prof. Diana Adlienė; Faculty of Mathematics and Natural Sciences, Kaunas University of Technology.

Research field and area: Biomedical Sciences, Medicine and Health.

Keywords: *Monte Carlo, simulation, brachytherapy, anthropomorphic head phantom*

Kaunas, 2017. 74 p.

SUMMARY

Monte Carlo (MC) code was used to simulate the dose distribution during the head-related brachytherapy procedures. The simulation was performed with Fluka code and a voxel-based anthropomorphic head phantom taken from original Zubal Phantom which contains 25 anatomical regions with medium specified to be equivalent to the different tissues accordingly ICRU reports. The results show that heterogeneous tissues with different densities and compositions such as bone, an air in the mouth cavity and sinuses, and other created the fluctuations and influenced the dose absorption. It may be stated that in the cases where the source is placed or travel near the tissues of very different density such as bone or air-filled mouth cavity or sinus region, it may result in distortion of dose distribution and contribute to the higher overall uncertainty if compared with the doses obtained using standard treatment planning system. The results of performed simulations are expected to be used in the clinical practice for the analysis and verification of dose treatment plans in order to achieve more precise brachytherapy treatment and reduce the dose uncertainties.

Ševčik, Aleksandras. Brachiterapijos dozių pasiskirstymo vokseliniame žmogaus galvos fantome modeliavimas Monte Karlo metodu. Magistro baigiamasis projektas / vadovė prof. Diana Adlienė; Kauno technologijos universitetas, Gamtos ir matematikos mokslų fakultetas.

Mokslo kryptis ir sritis: Biomedicinos mokslai, Medicina ir sveikata.

Reikšminiai žodžiai: *Monte Karlo modeliavimas, simuliacija, brachiterapija, vokselinis, žmogaus galvos anatominis fantomas.*

Kaunas, 2017. 74 p.

SANTRAUKA

Šiame projekte buvo atlikta brachiterapinio šaltinio dozės pasiskirstymo galvoje simuliacija naudojant Monte Karlo metodą. Modeliavimas buvo atliekamas su Monte Karlo kodo programiniu paketu FLUKA ir Zubal VoxelMan antropomorfiniu vokseliniu galvos fantomu, kuris turi 25 skirtingus anatomines sritis su atitinkamai priskirtais anatominių audinių ekvivalentais. Simuliacijų rezultatuose parodyta heterogeninio skirtingų audinių tankio ir cheminės sudėties įtaka dozės pasiskirstymui ir pateiktos vizualios fliuktuacijos. Nustatyta, kad šaltiniui esant šalia ypač skirtingo tankio sričių, tokių kaip kaulai arba sinusų ančiai, realus dozės pasiskirstymas nėra tapatus dozės pasiskirstymui, skaičiuojamam pagal TG-43 protokolą, šaltiniui esant homogeniškoje vandens aplinkoje. Gauti rezultatai bus naudojami tolesnei analizei, siekiant tikslesnio dozės pasiskirstymo brachiterapijos procedūrose, taip pat panaudojami dozės verifikacijai esant sudėtingiems klinikiniams atvejams, pavyzdžiui, pacientui su žandikaulio metaliniu implantu ar kitais metaliniais artefaktais paciento burnoje.

1. INTRODUCTION

The main objective of radiotherapy is to deliver the lethal dose to target cells with minimum harm to the adjacent tissues. The main advantage of brachytherapy method is an ability to induce less harm to the surrounding areas while ensuring the high energy delivery to the malignant tissues due to Inverse Square Law property applied for the radiation field. In such case, it is essential to know the dose distribution of the source with the most available accuracy. It is recommended in TG43U1[1] that the initial dose distribution data should be obtained either by experiment or by Monte Carlo (MC) simulation using appropriate code to ensure the exact dose delivery to the patient.

Current clinical systems calculate the dose of brachytherapy source taking the medium as homogenous water equivalent. It may be expected that accuracy of dose rate and distribution may suffer due to the induced fluctuations in dose absorption of the actual heterogeneous tissues with different densities and compositions such as bone, an air in the mouth cavity and sinuses, or artificial implants as such. In extreme cases where the source is placed or travel near the media of very different density, it may result in different doses as compared to the water phantom based (standard) doses and result in the higher overall uncertainty than recommended.

This work aims to simulate the dose inhomogeneities during the head and neck patient brachytherapy treatment procedures occurring due to different tissues like bone, soft tissues, an air in the mouth cavity and sinuses, and other. The results will be used for further analysis in order to achieve more precise brachytherapy treatment and reduce the dose uncertainties in the clinical practice.

Dose distributions around brachytherapy source placed in a certain region of a voxel-based anthropomorphic head phantom adjusted from original Zubal Phantom[2, 3] which contains 25 anatomical regions that are specified to be equivalent to the different tissues according to the ICRU reports[4, 5], have been modeled using MC simulation Fluka code[6, 7]. The series of simulations have been performed analyzing the dose distribution and comparing it with water equivalent. The main goal of the performed modeling was to accurately simulate the dose distribution of brachytherapy source in 3D anthropomorphic human head phantom containing anatomic regions with corresponding tissue compositions and to assess the possibilities of the method with the aim of its using as a verification tool in Quality Assurance (QA).

The work also comprises brief presentation of the current mathematical formalism of the dose evaluation during brachytherapy treatment according AAPM TG-43 report[8] and its updates[1] as well as the basics of MC method, mathematical formalism and the code used for the simulations.

2. LITERATURE OVERVIEW

2.1 Brief historical insight into the dosimetry of brachytherapy

The first procedures where radioactive nuclide was used for treatment of prostate cancer can be traced back to 1909[9], however, only in 1982 the actual increase of the procedures can be noticed. The reason for this is that earlier was no technical means to ensure and guide the effective and safe usage of radioisotope. Improvements in radioactive source designs, introduction of new technical equipment and imaging methods enabled to make the brachytherapy as a conventional radiotherapy procedure in the oncology.

The development of practical cavity theory[10] made a foundation for the technique to measure an exposure from radium sources. This system allowed to measure and calculates an exposure using ion chambers with sufficient wall thickness that enables charged-particle equilibrium. Later the achievements of computerized treatment planning and dosimetry methods in brachytherapy treatment planning enabled transfer from table-based systems to patient-specific 2D and 3D dose distributions. The NIST (the National Institutes of Standards and Technology) in the US announced the primary standards of reference exposure rate based upon carbon wall spherical ionization chambers for Cs-137 and Co-60 sources in 1974[11] and for Ir-192 brachytherapy sources in 1980[12]. By the 1990 the thermoluminescence dosimetry (TLD) was accepted as the most reliable and best validated experimental dosimetry in brachytherapy, mostly due to the efforts of collaborative work of the institutional group known as Interstitial Collaborative Working Group (ICWG)[13]. This group prepared the reference procedures for calibrating TLD detectors and recommendations for correcting the higher TLD response to low-energy photons as well as coefficients to estimate the absolute dose rates in water quantitatively.

Advancements in radiobiology as well as new technological improvements contributed further to the development of brachytherapy. The reference dosimetry protocols have been developed[8] by the joint collaboration of medical physicist teams under the lead of the American Association of Physicists in Medicine (AAPM) . For the dosimetry of brachytherapy sources, the AAPM Task Group 43 (TG43) has established improved dose calculation formalism[1] that allowed. It consists of such factors as the dose rate constant, a radial dose function, an anisotropy function, a geometry factor, an anisotropy factor and the air kerma strength in respect with actual source construction and geometry in addition to the primary photon spectrum. As from the issue of this report, the number of research publications related to the dosimetry in brachytherapy has grown substantially, documenting both improved dosimetry methodologies and dosimetric characterization of used source models.

The new step was taken with development of MC code for radiation transport. The first

brachytherapy dose distributions computed by MC method were published by Meisberger in 1960s who calculated 1D tissue-attenuation and scatter build-up factors for point sources of the most common radionuclides[14]. Low-energy ^{125}I radionuclide was analyzed by Dale in 1983 who was the first one to use a Monte Carlo computational technique to establish the certain tables of parameters dosimetry of the brachytherapy nuclide in a variety of tissues and organs[15] including the relation of the composition of a tissue with the dose absorbed at any location around the source. The commercial seed of the same ^{125}I radionuclide was simulated in 3D by Burns and Raeside[16]. The team modeled the seed submerged in a water phantom and calculated the dose rate per unit activity data expressed as a matrix surrounding the seed. Relative dose data were shown as 2D graph and compared with the reference data. Williamson's group in 1991 did the series of MC calculations of several radionuclides with high level of precision[17] . The experimental comparative measurements in water demonstrated that MC accurately reproduced the dose rates across the entire brachytherapy energy range in both homogeneous and heterogeneous phantom geometries[18] which confirmed that MC simulations are adequately accurate to support clinical dosimetry.

The interest to brachytherapy treatment and the challenges of its dosimetry increased the number of MC-related brachytherapy peer-reviewed papers[19] and recent simulations extend beyond the single source dosimetry with focus on patient-oriented applications.

2.2 Brachytherapy dose computation

The dose distribution around brachytherapy source depends on the emitted energy spectra, the geometry of the source and the surrounding material. The widely accepted dosimetry protocol, TG-43 report[1, 8] has been established by the American Association of Physicists in Medicine (AAPM) which assumes a water medium with superposition of single source dose distributions, no inter-source attenuation (ISA) effects, and full scatter conditions at dose calculation points. Complex source geometry and a number of factors involved make manual dose calculations very tiresome, so computational treatment planning systems (TPS) are used. Precise operation of TPS in source localization and dose computations is absolutely necessary to ensure planned dose delivery.

The most treatment planning systems use mathematical formalism provided in TG-43 protocol[1] The TPS apply the source superposition method to cylindrically symmetric photon emitting brachytherapy source in the clinically defined volume. The software is able to visualize the distribution of isodoses and dose volume histograms (DVH) within the defined regions of source locations. It is to notice that the dose distributions planned by conventional brachytherapy TPS fit well when source shielding is negligible, the media of the volume of interest is equivalent to water over the used energy range and no high-Z materials are present. The low energy sources

are especially sensitive to these conditions but the high energy sources such as ^{192}Ir may be treated in the same way to some extent.

In the case of brachytherapy, MC is perfectly suited to solve the complex problem of particle transport and energy deposition within a heterogeneous medium such as tissues of the human body. An extensive evaluation of the MC method in radiotherapy is given by DeMarco[20], Seco and Verhaegen[21] and references within.

The most established application of MC methods in brachytherapy is the determination of dose rate distributions around single radiation sources. While inverse square law dependence is the leading feature of brachytherapy dose distributions, photon attenuation and scatter build-up in the surrounding heterogeneous medium as well as particle interactions within the source assembly result in anisotropic dose distributions[22]. It is difficult to experimentally measure single-source dose distributions in brachytherapy due to the sharp dose gradients, low photon energies, and anisotropic dose rate curves. So the computational dosimetry techniques such as MC simulations became an crucial tool in brachytherapy[23]. MC simulations allow a proper accounting for radiobiological effects in low-energy brachytherapy which involves calculation of photon and electron spectra at various distances from sources.

Modern techniques are being developed that includes MC simulations to the some extent. Full MC simulation is not clinically feasible at the moment. The big efforts have been made to develop the MC dose calculation algorithms used in the TPS[24]. The main reason for this is a high computation power of multi-core computational systems that is required to gain viable simulations results. However MC codes are being utilized partly, merging pre-calculated Monte Carlo results and conventional TPS calculations and thus results obtained are usually more accurate than non-stochastic methods.

Several studies have compared MC dose calculations to the results of the TG-43 formalism analyzing different aspects of the dosimetrical quantities which are hard to measure experimentally, such as an impact of ISA[25], prostate implant geometries[26], tissue composition[27, 28] founding the deviations of the dose to tissue up to 35% in certain cases.

As example of such merge of two methods the new treatment planning technique called Tufts technique was presented by Rivard et al[29] in 2009 which may be applied in the clinical situations where the conventional approach is not adequate. Complex brachytherapy source configurations and their dose distributions from determined with Monte Carlo simulations were used as input data thus enabling new technique which uses conventional formalism adjusted with incorporated complex Monte Carlo-based brachytherapy dose distributions. In the result Rivard et al[29] indicates that "[...] time needed to calculate dose was less than 1 s in all cases since the complex dose distribution for one virtual source was precalculated during the virtual source commissioning

phase and data were stored in the TPS“ , It is also stated that this fast calculation technique deviate less than 1% from full MC results. In addition, this technique also can be applied to calculate dose to a specific tissue type instead of dose to liquid water.

There is a high interest of developing MC-based treatment planning software, mainly utilizing the same principle of fast MC code adaption combined with biasing techniques to achieve clinically feasible computation times: TPSDose43[30], RayStretch[31], egs_brachy[32], gBMC[33] and others. One of the earliest programs, so called an accelerated Monte Carlo code MCPI[34] was presented in 2006 for dose calculation in prostate brachytherapy. MCPI models a set of low energy seeds with specific positions in a 3D heterogeneous phantom representing the prostate and surrounding tissue. It uses a phase space data and a hybrid geometry model for treatment of the interseed attenuation and tissue heterogeneity effects. It is reported that MCPI needs 59 s (single 2.4 GHz Pentium 4 CPU) to perform dosimetry.

BrachyDose is a general purpose Monte Carlo code for rapid brachytherapy calculations presented by Yegin et[35] al in 2006. The code uses the general EGSnrc code system[36] and is based on Yegin's MultiGeometry[37] auxiliary package. The tool may simulate high energy sources such as ^{192}Ir as well as full dose calculations from the seed implants for treatment planning where many seeds exist in the geometry, including inter-seed and tissue inhomogeneities effects. Dose is calculated by scoring collision kerma using a tracklength estimator and special biasing techniques are applied to reduce the computational time. The technique does not require disk space to store a phase space file. For typical low energy brachytherapy applications with ^{125}I seeds, only 510 s were used to calculate complete 3D dose distribution in a 1x1x1 mm3 array of voxels with a 2% statistical uncertainty. In other experiment, it took less than 30 seconds in $(2\ mm)^3$ voxels on a single 3.0 GHz core[38]. Such results make it the program feasible in the clinical practice. In the benchmark with other methods, the calculations made with Brachydose show good agreement[39]. Further development of the software include graphical user interface (GUI) and data integration in the DICOM-RT format while working towards clinical implementation[38, 39]. Other researchers started to use it as well instead of original EGSnrc code[40].

Promising results were demonstrated with ALGEBRA[41], a Monte Carlo platform for dosimetry in brachytherapy which is based on the GEANT4[42] Monte Carlo code. It allows to place the source seeds in a realistic model of the patient made with appropriate chemical compositions and densities. Considering human tissues with different chemical compositions and densities different than water as well as interseed attenuation. the ALGEBRA is sufficiently fast and accurate for clinical and research purposes. ALGEBRA is developed as complete system fro brachytherapy dosimetry, that may use the DICOM RT formalism for image data handling and calculate the detailed dose distribution, consider the statistical uncertainties and create DVH for

the target. The calculation of the dose distribution takes around 12 min for a prostate case and in about 6 min for a breast case at 2% statistical uncertainty over a 2 × 2 × 2 mm3 mesh. It also enables to compare MC calculations with TG43 or any other DICOM compatible dose calculation. Further developments include a user-friendly GUI and HDR dosimetry as well as an automatic seed optimisation. Dose distributions can be extracted for visualization with, e.g., BrachyGUI[43] which allows to generate three views of patient images with two sets of isodose lines, and the ratio map of two dose distributions, including dose, uncertainty, dose difference, gamma index, CT number, density, or material map display (**fig.1**).

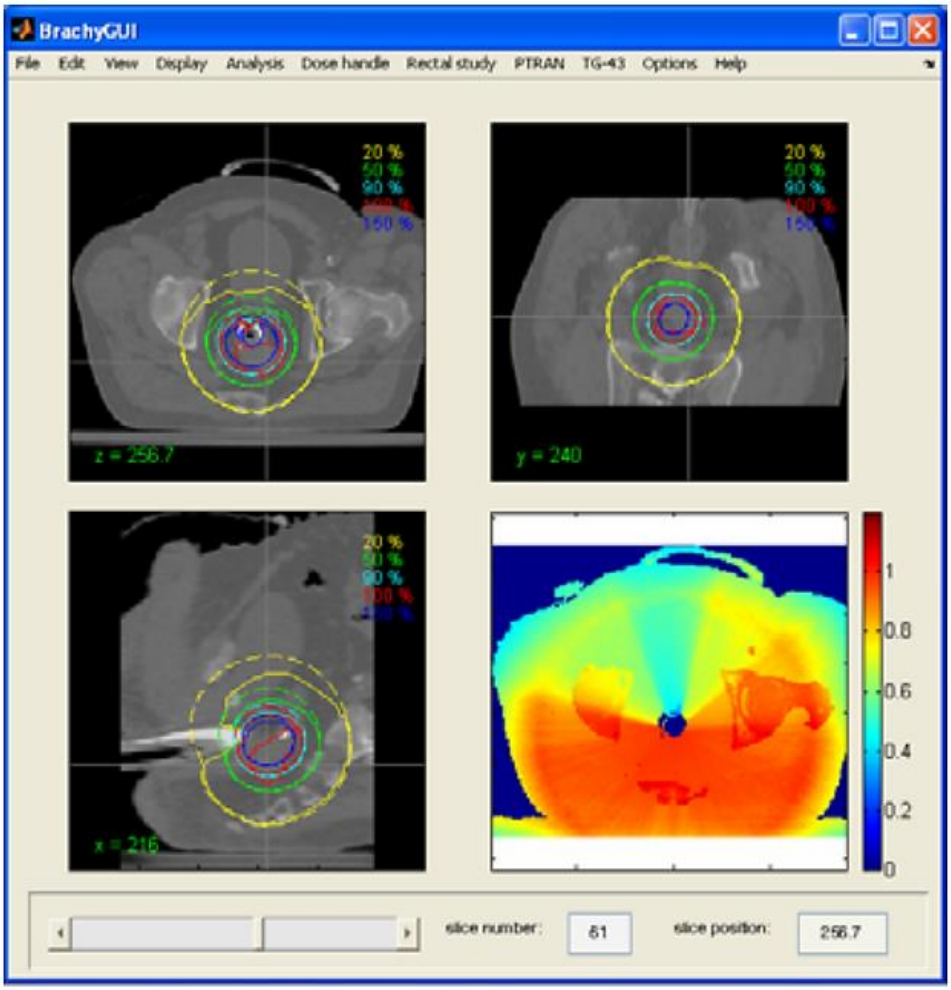

Figure 1. BrachyGUI visual interface[43]

However, by this day, despite being named as a reference dosimetry method for brachytherapy, MC has not been implemented in commercial TPS yet. In additional to TG-43 formalism, commercial TPS may use other methods as well, such as linear Boltzmann transport equation solver[44] and is implemented in Varian Medical Systems, Acuros™[45]. The newest version incorporated the option to calculate dose to voxel medium in the heterogeneous geometry using macroscopic kerma cross-sections to comply with TG186 recommendations[46].

Other methods of dose calculations in brachytherapy have been developed based on the collapsed cone superposition (CCS) algorithm. The collapsed cone algorithm is integrated to the Oncentra Brachy TPS from Elekta[47, 48] and being updated to satisfy the new requirements of TG-186 protocol.

To summarize, currently most treatment planning systems use TG-43 protocol adaptations with specific computational approaches. However, this protocol has limited accuracy in certain cases as neglecting tissue heterogeneity, scattered radiation as well as applicator attenuation so implementation of new brachytherapy protocol TG-186 is under way into the clinical practice in which patient-specific phantom is used and heterogeneities are considered.

Papagiannis et al[49] states that both clinically available model-based dose calculation algorithms attain a dosimetric accuracy improvement compared with TG43-based calculations yet the clinical benefit from improved accuracy remains to be evaluated. As for MC based software, at the moment it remains more as verification tool in the quality assurance (QA) systems then the actually utilized treatment planning software.

2.3 Verification in brachytherapy as part of Quality Assurance

The new technologies and methodologies evolve rapidly together with increased demand to quality and safety of the patient treatment. The advancements in radiobiology and new understanding of level of uncertainties in low-level radiation and its possible part of inducing the secondary cancers all together with increased technological improvement requires new level of QA procedures. The patient-specific dose calculations are on focus now due to new advances in understanding of complex radiobiological damage phenomena[50–52].

The verification may be done at various levels, from simple manual calculation of every dose distribution to check if the TPS output is reasonable from to selective MC simulation of chosen patient dose calculation to see if optimal dose distribution is achieved. The first one is run as a step to prevent gross errors of human factor or system failure. With advancement in treatment technology using sophisticated dose optimization software, it has become a puzzling task to verify optimized dose delivery to prevent any gross errors in TPS output[53]. The Nuclear Regulatory Commission states that a difference of 20% between the prescribed total dose and directed total dose to be a reportable medical event[54].

From a wider perspective the complex specifically chosen verification using MC simulation with included additional factors such as region boundary or different tissues may be seen as a part of continuous improvement in dose optimization protocols. The principle of continuous improvement is one of the core foundations of modern Quality Management Systems (QMS).

It is stated in Euratom Directive 2013/59 that “For all medical exposure of patients for

radiotherapeutic purposes, exposures of target volumes shall be individually planned and their delivery appropriately verified taking into account that doses to non-target volumes and tissues shall be as low as reasonably achievable and consistent with the intended radiotherapeutic purpose of the exposure"[55]. This statement which is part of the optimization principle gives a basis for foundation of a patient-specific dosimetry. The new branches of radiotherapy emerge such as molecular radiotherapy[56–58] with focus to indvidualize the dose to each person specifically according genetical and other factors.

It is mandatory for clinical applications that the dose distribution inside a patient should be evaluated and verified, which includes the non-point source configuration as well as attenuation and scattering of the radiation within the tissue. The dose distribution which is based only on the mathematical formulism are often limited. Actual brachytherapy sources are rarely spherical in structure and exhibit anisotropy due to self-attenuation of the radiation inside the source. Therefore the assumption that the radiation is isotopically produced around the source may lead to significant errors by neglecting the anisotropy of the source.

New technologies come to clinical practice such as real-time ultrasound guidance for brachytherapy, on-line imaging with ability to generate dose distribution delivered to the patient, real-time reoptimization of treatment plans with possibility of four-dimensional dose calculations to determine the actual dose delivered to tissue voxels. Combined with the principal need of optimization of radiation, a strong QA culture is essential. Verification of the dose delivered is an extremely important step in QA system which should become a daily routine in every institution. It also must be ensured that new systems are developed with verification methodology described as a part of the clinical implementation process. It may be firmly stated that in order to ensure the optimal treatment of patients, an institution must develop a suitable QA program for brachytherapy sources, equipment and the clinical procedures

The verification is an essential part of QA and has a requirement to be independent. Independent verification by two different protocols assures the quality of treatment. This should always be practiced to increase the accuracy of treatment even it's time consuming practice[59]. The verification can be utilized by various means: using mathematical formulism, experimentally or using computational simulation software. Confirmation of the accuracy of optimized calculations with verification evaluation technique is vital in order to assure the accuracy of treatment[59].

2.4 Verification by mathematical formulism

Most of verifications proposed utilized some sort of mathematical formulism and are based on certain equations. The main purpose for such verification usually are protection from human errors

and miscalculations but it's rarely include other factors which was not included in pre-treatment dose calculation.

However in special cases there is a need for quick manual check of TPS output to avert systematic errors. In such cases the manual dose verifications may be used. This is especially true during commissioning after loading brachytherapy unit, where it is a requirement to include manual dose verification of TPS results[53]. As an example, a quick mathematical method to verify the computational accuracy within 10% is given by Shanta[53]:

$$D_{point} = \frac{S_K \cdot f_{(ak,wat)} \cdot WPF_{ri} \cdot t}{r^2}, \qquad (1)$$

where

S_k – the source strength specified in air kerma strength,

WPF – the water perturbation factor (also referred to as Tissue Air Ratio),

r – the distance (in cm) from the center of the active source to the point of interest,

t – the duration of treatment,

f(ak,wat) – the air kerma to dose in water conversion factor.

As an additional example, the quick and easy independent verification check is proposed by Gadhi et al[60] to verify the output of TPS ABACUS 3.1 for the treatment of high dose rate intraluminal brachytherapy. The manual calculation deviates from the TPS result up to 2% only and may be used to enhance the reliability of brachytherapy treatment as a part of QA check to identify human error-related planning inaccuracies. The mathematical expression is simple and could be used for every procedure without use of much time. The author especially underlines that simplicity of technique claiming that no particular expertise is needed. The verification takes about one minute and does not significantly lengthen the patient's waiting time. It does not have an objective to optimize the prescribed dose but rather preventing the human or machine errors during periodic QA tests and serves as an independent safety layer.

There are many papers proposing the various techniques of manual mathematical verifications of TPS output during the brachytherapy procedures. They may be provided not only as mathematical formulas but may be developed based on workbooks/spreadsheets as well to simplify the verification itself and reduce its time. The more complex mathematical verification methods are proposed as software packages, but all of them mostly follow the TG-43 formalism and software package itself is for convenience and time-saving purposes[61–63].

2.5 Experimental verification

The other means of brachytherapy dose verification is an experimental way in which the actual dosimeters are used, usually a set of thermoluminescence dosimeters (TLD). A good example of it is a case study done by Nikoofar et al[64]. The dosimeters were put in an anthropomorphic phantom constructed from natural bone and mixture of paraffin wax with sodium chloride. TLDs were placed in several depths in and around oesophagus. CT scans were used to avoid any discrepancy between the planned and the treated phantom set-up. In the paper it actually confirmed that dose distribution around sources not only was depended on distance from source and its size, but also was related to the tissues absorption and scattering. Several similar verification procedures using TLD are proposed[65–68] including in-vivo TLD dosimetry[69, 70].

There is reported successful use of MOSFET dosimeter and diamond detector uses for the same purpose[71]. The dosimeter readings take at up to twelve locations on the surface in an anthropomorphic phantom. It also allows to place an array of dosimeters on the patient's skin verify the position in three-dimensions. In addition, the semiconductor properties allowed to automate process together with a mathematical algorithm which was made to evaluate the location of the source given a measured data set with contribution of tissue inhomogeneity. This study proposes the real-time system to verify brachytherapy procedure in vivo.

Other experimental methods include the use of radiochromic film[72] and ionization chambers[73] as well as spectroscopic dosimetry[74, 75].

Chemical dosimetry takes a part of the methods that are used for dose measuring during the brachytherapy procedures. The polymer gel dosimeters have a real potential of the dose verification when complex irradiation regimes with multiple sources are involved in the specific geometry[76–79]. Gel dosimeters are made from radiation sensitive material which polymerize as a function of the absorbed radiation dose. They have the capacity to image radiation dose distribution in 3D. Various accuracies are reported. Vandecasteele[76] reports that gel dosimetry allows to measure the absolute dose in the whole 3D volume within 5% accuracy. Comparison study by Senkesen et al[80] concludes that good agreement between the gel dosimetry and TPS results is achieved and may be used for HDR brachytherapy sources and 3D dose verification. In 2006 the solid polymeric dosimeter (SPD), was commercialized as PRESAGE[76]. However, it must be noted that chemical dosimeters do not quantify the absorbed energy but rather count on expected relationship between the absorbed dose and the amount of the volumetric change of the dosimeter medium[81]. Therefore the main use of 3D dosimeters is the validation of the dose delivery and volumetric effect in comparison of the 3D dose distributions planned by the TPS.

2.6 Verification by MC simulation software

There are constant studies that note MC code as Quality Assurance QA tool[82]. The main general MC packages commonly used in the medical physics are MCNP, EGS4, EGSnrc, GEANT4, PENELOPE and FLUKA. The EGS4/EGSnrc codes especially very much used in the radiotherapy and dosimetry, representing a de facto standard for photon–electron transport in the energy range (1 ÷ 10 MeV) of radiotherapy interest[83].

MCNP[84] is a general-purpose Monte Carlo code that can be used for neutron, photon, and electron or coupled neutron/ photon/electron transport with very extended and powerful capabilities. A broad collection of cross-section data MCNP is developed and maintained at Los Alamos National Laboratory. Extremely wide applications almost in every case of the medical physics field is possible, including but not limited to any kind of shielding calculations, dose distributions, neutron and heavy particle interaction simulations, radio immunotherapy and boron neutron capture therapy, X-ray computed tomography and positron emission tomography simulations, many applications in nuclear medicine, etc. MCNP code is a leader used currently in such studies as dosimetry perturbations of the source within high-Z materials[85], dose distribution of difference media[86] or the update of treatment planning systems with more innovative dose calculation including patient-specific scatter and material heterogeneity conditions[87].

The Electron Gamma Shower (EGS4)[88] is a general purpose MC package able to simulate energies from a few keV up to several TeV. Originally developed at Stanford Linear Accelerator Center, USA for high energy physics applications, it has been extended to be applied for lower energy applications. EGSnrc[36, 88] is an upgraded version of the EGS4 package. It is freely available for scientific community.

The GEANT[42] was originally designed for high energy physics experiments in the CERN, but later was adjusted for the areas of medical and biological sciences, radiation protection and astronautics. The code may simulate electrons, positrons, γ-rays, X-rays, optical photons and muon interactions, as well as hadrons and ions interactions. However, it is toolkit, not the tool, and the extensive knowledge of the code as well as good C++ programming skills should be presented in order to use it successfully.

PENELOPE[89], Penetration and ENErgy LOss of Positrons and Electrons, is well known MC code mainly used for radiotherapy, dosimetry and nuclear medicine. It is capable of simulating all kinds of interactions (except nuclear) from 50 eV to 10^9 eV. It is freely distributed for scientific purpose. PENELOPE uses a pure class II (mixed) algorithm for electrons/positrons which gives

the constancy under variation of simulation parameters.

FLUKA code is briefly presented in chapter 3.7.

The new MC codes are being developed currently such as GPU-based Monte Carlo dose calculation code DPM[90, 91], which allows to reduce the calculation time significantly, up to 5 to 7 times. However, there seems to be much more possibility in the using GPU architecture for MC calculations. As reported in the other research of GPU based MC code GPUMCD presented by Hissoiny et al[92], GPUMCD is more than 900 times faster than EGSnrc in terms of simulation speed.

Being named as the most accurate simulation method MC is often used as a reference method to verify the dose distribution. The simulation gives the flexibility to include various parameters such as different media properties and complex geometries and is equivalent to the experiment itself due to the stochastic nature of the radiation itself. However, the method itself is subject to type A uncertainties in addition to type B and requires a lot of computational time which makes it clinically unfeasible. The various biasing options, however, enable to utilize MC simulation accuracy within reasonable times and provide the possibilities to use MC not only for verification but for treatment planning as well (see chapter 2.2 in this project for more details).

The question remains if analogue MC simulation may be still useful for dose calculation. While certainly not feasible in everyday clinical practise, it may have a benefit in case of complex cases such as patient with artificial jawbone where much of uncertainty is present. The unbiased analogue MC simulation yet takes a huge amount of time but allows to be used as “black box” with care. Analogue Monte Carlo samples for actual phase space distributions and gives a prediction of all statistical moments of any order and average quantities. In addition, it preserves correlations and reproduces fluctuations in the most accurate way.

Referring to this project, we see the potential of analogue unbiased MC simulation to be used as verification in the specific cases with complex geometry or high-Z materials are present. While specifically developed MC based software have limited flexibility, it is possible to utilize analogue MC simulations to get additional data for verification. Exemplary case of such event would be a patient with artificial jawbone having a head-neck cancer.

However, it should be pointed out that with improvements of GPU based MC codes the future of MC clinical use belongs to them due to unmatched efficiency and calculation speed.

2.7 Computational phantoms

Patient-oriented applications have an inherent need of anthropomorphic computational phantoms. From the phantoms based on simple quadratic equations in 1960s to voxelized phantoms based on actual medical images of the human body today is a major step that opens

many of new possibilities for the applications. Even the very first generation of MIRD phantom[93] gave the new insights for the dose calculation for individual organ (**fig. 2**).

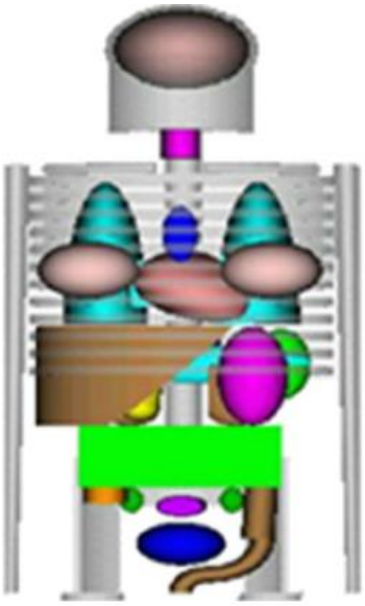

Figure 2. The original MIRD phantom[94]

Large degree of error and limited accuracy was an issue using such phantoms. The next generation could not come before the improved computer technology took the place. The actual breakthrough happened when computed tomography (CT) and magnetic resonance imaging (MRI) devices could create the accurate images of internal organs in 3D. This diagnostic data have been transformed into a voxel format enabling to reproduce the human body in digital form. More than 38 phantoms today are available worldwide for different uses[95].

Zubal and team at Yale University developed the VoxelMan phantom[2, 3, 96] in 1994. The part of it is used in this project. The original phantom was created from head-to-torso and intended for improving nuclear medicine. Transmission computerized x-ray tomography (CT) was used to get the high resolution 3-dimensional human anatomy essential to construct the volume segmented phantom. Organ frameworks were manually drawn with millimetre resolution in each of 129 transverse slice images of the human torso (**fig. 3**). After the data has been set, the slices were transformed to get symmetric voxels of 4 mm, using a median compression scheme.

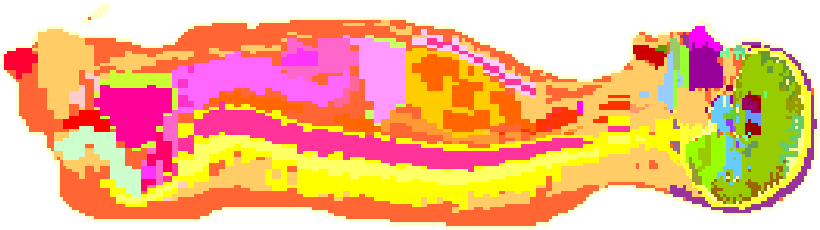

Figure 3. The slice of Zubal VoxelMan (taken from[97])

The third generation phantoms have become available, so called boundary representation phantoms which computational human models that contain anatomical structures of a human body using boundary representation method. Design of this type of phantom is realized by Non-Uniform Rational B-Spline method or polygonal mesh method, which are usually collectively called BREP methods[98]. BREP phantoms are better suited for geometry deformation and adjustment in comparison to the voxel phantoms, and allow the morphing into an existing reference phantom or into the anatomy of a real patient for the calculation of individual-specific dose calculation (**fig.4**).

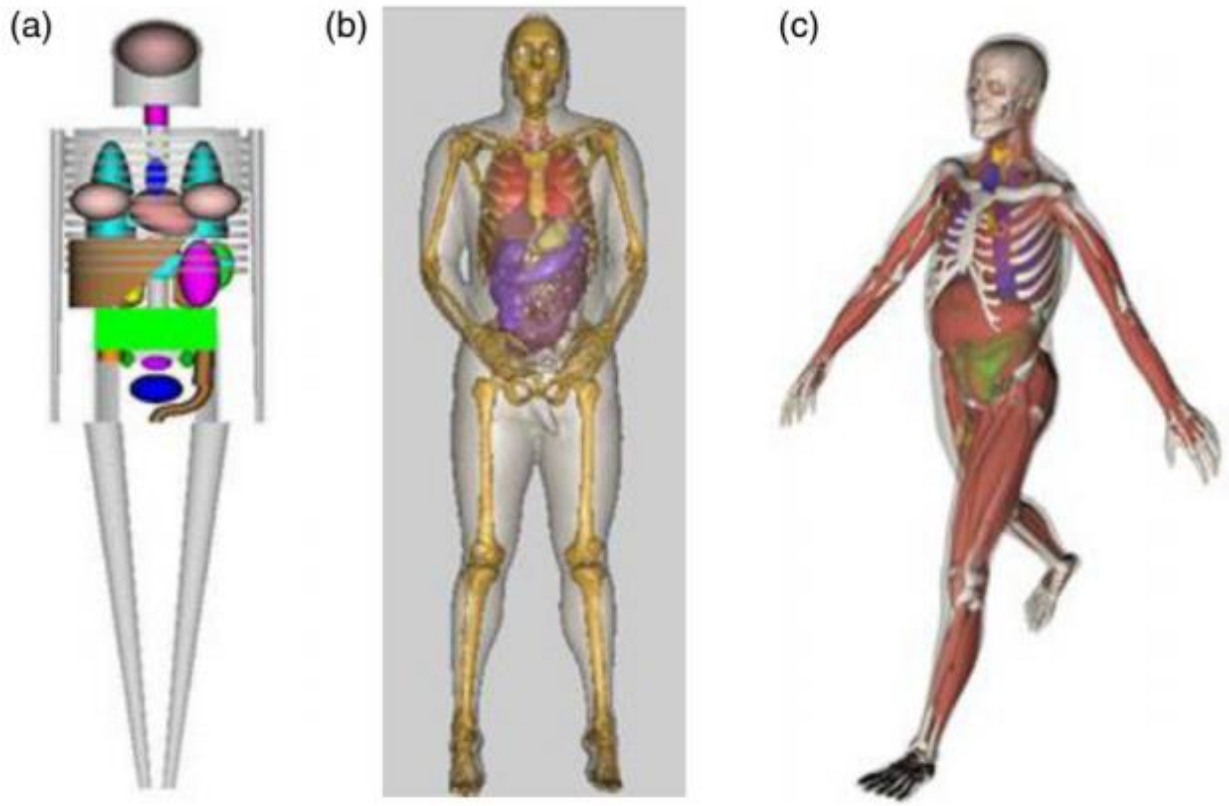

Figure 4. Three phantom generations: (a) Stylized phantom; (b) Voxel phantom (but displayed in smooth surfaces); (c) BREP phantom (taken from[99])

2.8 State of the art research in the 3D MC simulations of brachytherapy using voxelized phantoms and FLUKA

Patient-specific dose calculations is on focus today and MC simulations are anticipated to improve the current methodology using TG-43-style table-based source-superposition algorithms[19]. The effective utilization of MC simulations in a common clinical practice would allow including the effect of interseed attenuation (ISA) and tissue heterogeneities for low-energy seed and applicator shielding and boundary scattering effects for higher-energy brachytherapy routines.

Heterogeneity of the tissues and possible impact of the additional materials such as implants are on the focus now. When comes to anthropomorphic voxel phantoms, relevant for this project is the work of Abella and Miro where they calculated 3D dose distribution calculation in a voxelized human phantom for the external beam therapy[100] and especially the study of prostate brachytherapy using the similar phantoms by Furtado et al[101]. However, the results are presented as Dose Volume Histogram (DHV) and not directly comparable to our brachytherapy project.

Searches for the recent papers using FLUKA code with keyword for brachytherapy do not give many results. Just recently a feasibility study for beta-emitting brachytherapy source using FLUKA code was released by Anjomrouz et[102] with positive evaluation. It can be seen that the code has mostly been dedicated to heavy ion therapy[103–106], radiation protection[107–109] and particle physics[110–112]. However, the recent improvements and future plans show that FLUKA intends to rise its popularity within the medical field beyond hadron therapy[113–116].

In general, the most of simulations are run for detail dosimetrical characteristics of sources in the various environments. The main code used for the simulations is MCNP while FLUKA is used rarely at the moment.We could not found comparative studies that would embrace the brachytherapy source inside the 3D voxelised anthropomorphic human phantom with assigned tissue equivalents and would show results in 3D.

2.9 Objective and tasks

All of above, the resulting objective is to use Monte Carlo (MC) package to accurately simulate the dose distribution of brachytherapy source placed in a certain position of 3D voxelised anthropomorphic human head phantom taking into account corresponding tissue compositions in the region of interest and evaluation of discrepancies between the dose values obtained from homogeneous media phantom and from modified heterogeneous media phantom calculations.

The objective will be achieved through the following tasks:

1) Set-up and run the initial simulations of ^{192}Ir brachytherapy source in the water and air sphere for the check-up;

2) Modification of Zubal VoxelMan phantom[2, 3, 96] and transformation of it into the FLUKA-ready geometry file;
3) Set-up and run the simulation of the source inside the tongue of the phantom when media of the regions are selected as water;
4) Set-up and run the simulation of the source inside the tongue of the phantom when media of the regions are selected as anatomically-equivalent;

3. MATERIALS AND METHODS

3.1 Background

A Monte Carlo simulation is based on repeated random sampling from probability

distributions representing the possible physical interactions applicable for the simulation. The independently simulated histories are summed up and post-processed to a numerical solution of the problem on the basis of the defined geometry, materials and the cross sections for the relevant interactions.

However, due to the complexity and required calculation time the method is not yet feasible for daily treatment planning in the clinics and typical TPS are using faster algorithms and derivations from MC for the daily basis. These systems are using certain assumptions such as unified material averaging the planning phantom geometry which is water in the most cases.

As it was stated above, there is a certain motivation to have the dose distribution as accurate as possible for the brachytherapy procedures. The human head consists of heterogeneous materials with different densities and compositions, and some areas such as mouth cavity or air-filled sinuses may be influencing dose distribution significantly.

This work simulates the dose distribution of Ir-192 source placed in the anthropomorphic head phantom region representing the middle of tongue. We intend to run the comparative simulations with (1) the phantom head consists of water only and (2) the phantom head consists of anatomically equivalent tissue compounds.

3.2 TG-43 formalism of dosimetry in brachytherapy

The dose distribution of a brachytherapy source is a complex function of the emitting energy spectra, the geometry of the source and the surrounding material. The widely accepted dosimetry protocol has been established by the AAPM TG-43 reports[1, 8].

The TG-43 formalism adopts a water medium with superposition of single source dose distributions, no ISA effects, and full scatter conditions (infinite or unbounded water medium) at dose calculation points.

The radial dose fall-off from any gamma source, the rate at which dose decreases with increasing distance from the source can be described by general 2D formalism given in the mentioned report:

(2)

r – distance (in cm) from the center of the active source to the point of interest,

r_0 – denotes the reference distance which is specified to be 1 cm,

θ – polar angle specifying the point of interest, P r, θ, relative to the source longitudinal axis, θ_0 – reference plane defines the source transverse plane, and is specified to 90°,

S_k – source strength specified in air kerma strength,

Λ – dose rate constant defined as the ratio of the dose rate at the reference point; the dose rate constant can be evaluated by using a calculation method such as the Monte Carlo method,

$G_x(r,\theta)$ – geometry function that describes the effect of the active source material distribution within the source on the dose distribution outside the source,

$g_x(r)$ – radial dose function accounting for the effects of absorption and scatter on the dose distribution in the medium along the transverse axis of the source,

$F(r,\theta)$ – anisotropy factor describes the effects of anisotropic photon attenuation.

Calculation of the dose rate of encapsulated cylindrical source (**fig.5**), at point $P(r,\theta) = P(x,y)$ relative to the source center is shown in the figure below.

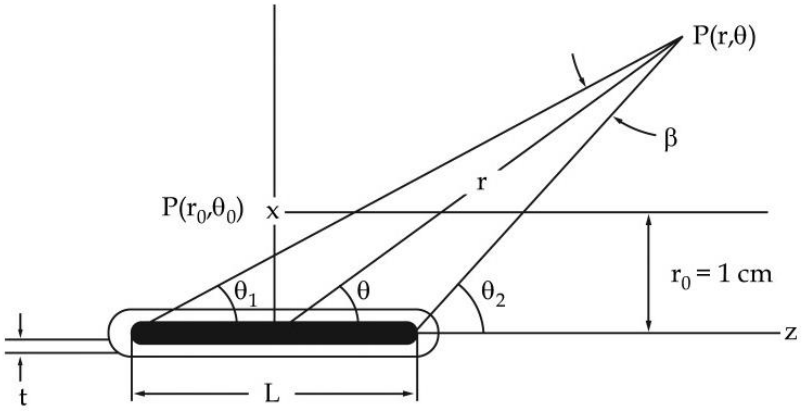

Figure 5. Coordinate system for brachytherapy dosimetry[1]

The dose-rate constant in water, Λ, depends on both the radionuclide and source model. It is the ratio of dose rate at reference position $D(r_0, \theta_0)$, and S_K:

$$\Lambda = \frac{D(r_0,\theta_0)}{S_K}, \tag{3}$$

where S_K represents air-kerma strength defined as the air-kerma rate $K_\delta(d)$ *in vacuo* at distance from the source center to the point of air-kerma specification:

$$S_K = K_\delta(d)d^2 \tag{4}$$

The geometry function is added to increase the accuracy with which dose rates can be projected by interpolation from data formulated at discrete points. It disregards scattering and attenuation, and is based on an effective inverse square-law correction using selected geometry

model of the spatial distribution of radioactivity within the source. Two main models are recommended to be used for the geometry functions: point-source approximation and line-source approximation[1].

The radial dose function, $g_X(r)$, accounts for dose fall-off on the transverse-plane due to photon scattering and attenuation, and is defined by eq. 4:

$$g_X(r) = \frac{D(r,\theta_0)}{D(r_0,\theta_0)} \frac{G_X(r_0,\theta_0)}{G_X(r,\theta_0)} \tag{5}$$

The 2D anisotropy function describes the variation in dose as a function of polar angle relative to the transverse plane.

$$F(r,\theta) = \frac{D(r,\theta)}{D(r,\theta_0)} \frac{G_L(r,\theta_0)}{G_L(r,\theta)} \tag{6}$$

The complex 2D dose distribution is approximated then to 1D isotropic point-source equation:

$$D(r) = S_k \Lambda \frac{G_X(r,\theta r}{G_X(r_0,\theta_0)} g_X(r) \cdot \phi_{an}(r) \tag{7}$$

The most treatment planning systems use the implementations of eq.8[1]:

$$D(r) = S_k \Lambda \cdot \left(\frac{r_0}{r}\right)^2 g_p(r) \cdot \phi_{an}(r) \tag{8}$$

3.3 Basics of Monte Carlo simulation

MC techniques are broadly used in natural sciences, including medical physics. It may be defined as a numerical method to solve equations or to calculate integrals based on random number sampling[19]. In general, we may state that we want to use this method to solve the problem of particle transport.

The Monte Carlo simulation of a given experimental arrangement involves the numerical generation of random histories. To simulate these histories “interaction model” is needed, i.e., a set of differential cross sections for the relevant interaction mechanisms. These cross sections determine the probability distribution functions (PDF) of the random variables that describe a track;

- free path between successive interaction events,
- type of interaction taking place,
- energy loss and angular deflection in a particular event,
- initial state of emitted secondary particles, if any

Once these PDFs are known, random histories can be generated by using suitable sampling methods. If the number of generated histories is large enough, by the law of large numbers quantitative information on the transport process may be obtained by simply averaging over the simulated histories

The concept of phase space is used to describe the mathematics of particle transport[119]. A phase space of a dynamical system is a space in which all possible states of a system are represented, with each possible state corresponding to one unique point. Each phase space dimension corresponds to a particle degree of freedom. Generally three dimensions correspond to position in real space, another three dimensions represent the moment of the particle, the other dimensions is the particle type itself, evolution time, quantum numbers, etc. Each particle is represented by a point in a phase space, and the overall number of particles in an infinitesimal phase-space region can be expressed:

$$dN = f(x, p, t, \alpha) d^3 p d^3 x dt d^n \alpha \qquad (8)$$

where *f* is a probability density function.

Particle transport is represented by the evolution of $f(x,p,t,\alpha)$ due to due to transport, scattering, particle absorption, decay, external forces, particle production, etc.[120]. This evolution is described by Boltzmann's transport equation[121]. It is an equilibrium equation in phase space: at any phase space point, the increment of angular flux Ψ in an infinitesimal phase space volume is equal to sum of all entering particles minus sum of all leaving particles. If we name the initial particle distribution function in a given phase space region as source, while a phase space region where the modified $f(x,p,t,\alpha)$ is to be calculated is to be a detector, the solution can be written as:

$$f(x, p, t, \alpha) = \iiint G(x, p, \alpha, x', p', \alpha') f_0(x', p', \alpha') d^3 p' d^3 x' d^n \alpha' \qquad (9)$$

where G s a multi-dimensional operator that includes all the microscopic processes.

It may be seen as the solution of any particle transport problem is a multi-dimensional integral in which all processes are described by probability distributions. The simplest solution can be written as an integral of $f(x,p,t,\alpha)$ over the region of interest:

$$N = \iiint_{\Delta p \Delta x \Delta \alpha} f(x, p, t, \alpha) d^3 p d^3 x d^n \alpha \qquad (10)$$

The solution of the actual problem involving scattering, absorption, various interactions, etc. involves complex integrations in many variables and makes a numerical solution hardly achievable. Multidimensional numerical integration is required to solve the system of coupled transport equations for problems in radiation therapy, for example, for dose calculation, and

similar.

MC method can be seen as an integration method that allows Msolving multi-dimensional integrals by sampling from a suitable stochastic distribution. The main idea of MC simulation is to use random samples of parameters or inputs to analyze the behavior of a complex system or process. The mathematical foundation of this method is central limit theorem (CLT) which states the arithmetic mean of a sufficiently large number of iterates of independent random variables, each with finite expected value and finite variance, will be approximately normally distributed[122]. In other words, given any observable X, that can be expressed as the result of a convolution of random processes, the average value of X can be obtained by sampling many values of X according to the probability distributions of the random processes.

The accuracy of MC estimator depends on the number of samples:

$$\sigma \propto \frac{1}{\sqrt{N}} \tag{11}$$

Random sampling from probability distributions of the outcome of physical events is the base of MC integration ensured by use of pseudo-random numbers which are sequences that reproduce the uniform distribution generated from mathematical algorithms. Various sampling methods are used then to obtain the values.

Particle transport tens itself naturally to be simulated by Monte Carlo being a physical process described by probabilities (the particle cross sections are equal to the interaction probabilities per unit distance). It is a system of equations because the transport problem for photons, electrons and other particles must be solved. For the most cases of radiation therapy we are interested in electron (positron) and the photon transport including the interactions (bremsstrahlung, Compton scatter, photo electric absorption, pair production, etc.). Practically the parameter space is limited because the region of importance is limited the simulation is stopped if the photon or electron energy falls below some minimum energy.

Radiation transport through radioactive decay is a complex process which includes but is not limited to of attenuation and scattering of photons, carriage of beta rays and secondary electrons via elastic and inelastic collisions with orbital electrons including bremsstrahlung.

The whole particle history (**fig. 6**) is simulated including all secondary particles and its daughter particles.

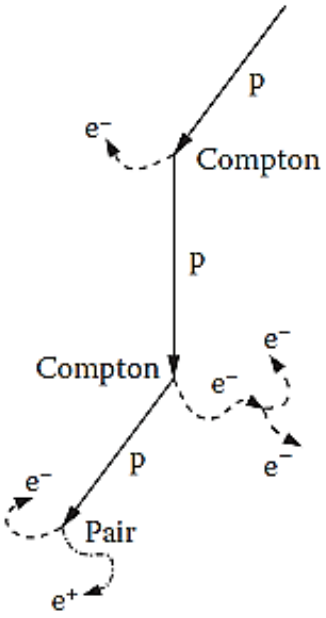

Figure 6. Example of a particle history starting with a primary photon via Compton interactions and pair production events leading to secondary products[19]

The transport simulation of a particle discontinues if it leaves the geometry of interest or its energy falls below some predefined minimum energy o so called cut-off parameters. In the energy range of radiation therapy the processes of photoelectric absorption, Raleigh scatter, Compton scatter, and pair production are mostly relevant[19] .In every step through the simulation the certain values are calculated for accumulation, for example, the dose is calculated integrating the values of absorbed energy per voxel.

However, such even-by-event simulation is not suitable for charged particles like electrons or protons which undergo a very large number of single interactions. It means that the simulation of one electron history would require an unfeasibly long calculation time. The certain method is applied called Condense History (CH) technique which was introduced in 1963 by Berger[123]. It is based on the assumption that almost all of charged particle interactions are elastic or semi elastic and only a tiny amount of energy is transferred from the charged particle to the surrounding matter on each interaction. In addition, the particle path angle changes in general only by small scattering angles and therefore it is possible to group many of these similar events into one CH step, where the direction change of the particle is simulated by one large multiple scattering angle[124]. The most of MC algorithms perform electron, positron, proton, or heavier charged particle transport using the CH technique (**fig. 7**).

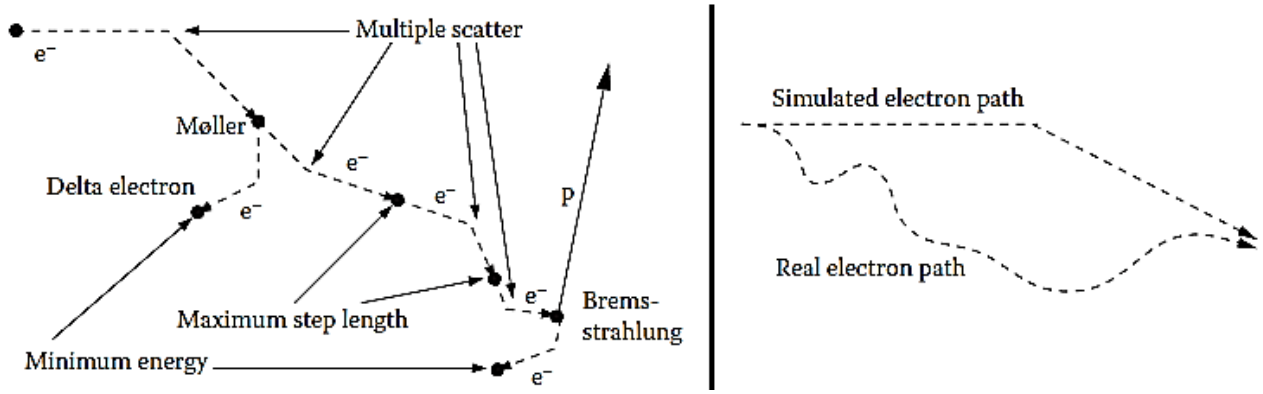

Figure 7. Example of a particle history starting with a primary electron (left side). In the right side the approximation of particle direction using the CH technique and path length corrections. Adapted from[19]

Photon interactions may also be simplified, for example, it is possible to model K-edge characteristic x-rays, but not consider L-edge x-rays for low-Z elements[125]. Also it must be noted that radiological interactions at energies less than a few keV will be highly influenced by molecular binding effects, which are not accounted for in most current MC codes in use[19].

Finally the suitable cross-section tables must be chosen and assigned to each material in the simulation geometry. The modern cross-section data are based on quantum mechanical models of each scattering and absorption process. The approximate models of orbital electron wave functions are used, with validation from available experimental measurements[126].

3.4 Geometry and material of the simulation

The TG-43 dose calculation formalism disregards patient tissue composition and is based upon specification of absorbed dose and transport of radiation in liquid water. The AAPM TG-43U1[1] report specifies liquid water to consist of exactly two parts hydrogen and one part oxygen with a mass density of 0.998 g/cm^3 at a temperature of 22°C. However, it may be assumed that significant deviation between expected in delivered dose, especially for low-energy sources due to the patient tissue compositions, densities, and dimensions which differs from the reference geometry.

The linear attenuation coefficient μ is related to ρ, so the density differences between water and human tissues will result in different photon energy fluence and dose distributions. As μ/ρ is larger at low photon energies, alterations of elemental composition will result in higher dose differences for low-energy sources[127].

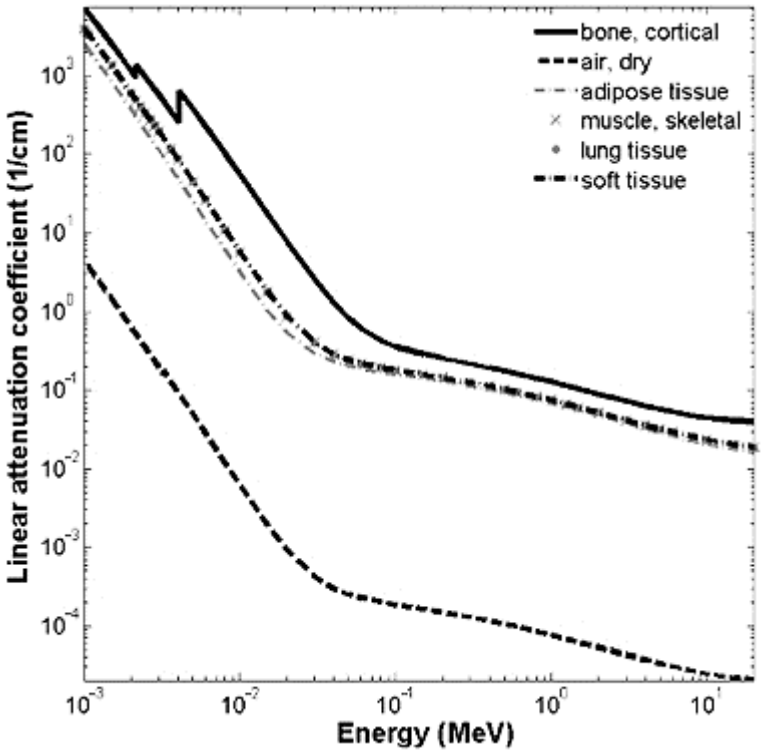

Figure 8. Linear attenuation coefficient for different absorbing mediums[128]

The AAPM TG-186[129] is the systematic attempt to formulate guidelines for assigning cross sections and densities where it states that all-water approximation for dose calculations may considerably deviate at low (E < 50 keV) and intermediate (50 keV < E < 200 keV) and are critical for electronic sources where mean photon energies are generally about 30 keV.

The typical geometry used in the simulation of single-source brachytherapy dose distributions is a liquid water sphere of radius 15 cm for low energy sources[1] and 40 cm for higher energy sources[130]. This represent doses in unbounded water medium over the clinically relevant distance range yet full scatter conditions are not met. It may be assumed that sources close to the skin will result in deviation of delivered dose[21].

3.5 ^{192}Ir radionuclide in brachytherapy

Main characteristics of a radionuclide used in the brachytherapy can be described:

- By its half-life – the time required for a quantity to reduce to half its initial value;
- By its specific activity – decays per time unit per quantity of atoms;
- By its energy spectrum – the energies that are emitted from the source.

Typical values of ^{192}Ir radionuclide used in the brachytherapy are given in the **table 1**.

The radionuclide is produced from enriched ^{191}Ir targets (37% natural abundance) in a reactor by the (n, γ) reaction, creating^{192}Ir sources (typically 1 mm diameter by 3.5 mm length cylinders) with activities exceeding 4.4 TBq[130]. HDR ^{192}Ir sources are encapsulated to ensure containment of the radioactive material and serve as a filter of unwanted radiation from beta rays produced through

the source decay of ^{192}Ir (**fig.9**).

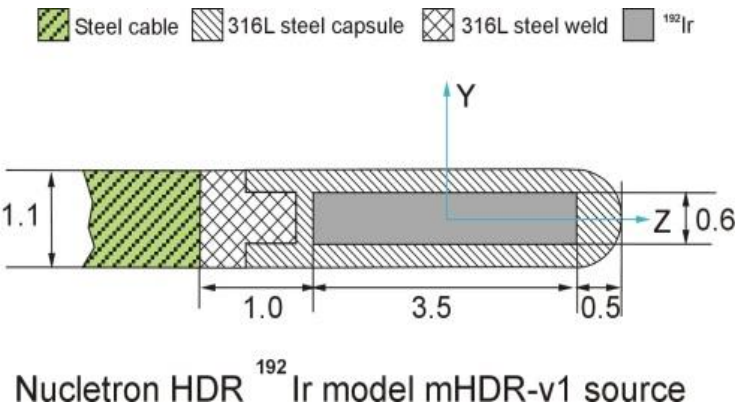

Figure 9.Ir-192 source encapsulation[130]

Table 1. Physical properties of Ir-192 radionuclide (adapted from[130])

Half-life	73.81 days
Type of disintegration	β^- (95.1%), EC (4.9%)
Maximum x-ray energy (keV)	78.6
Gamma energy-range (keV)	110.4–1378.2
Mean x-ray and gamma energy (keV)	350.0
Maximum β^- ray energies (keV)	81.7 (0.103%) 258.7 (5.6%) 538.8 (41.43%) 675.1 (48.0%)
Mean β^- ray energy (keV)	180.7
Air-kerma rate constant, $\Gamma_{\delta=10\ \mathrm{keV}}$ (μGy m^2 h^{-1} MBq^{-1})	0.1091
Specific activity (GBq mg^{-1})	341.0

3.6 FLUKA code

Monte Carlo code FLUktuierende KAskade (FLUKA)[6, 131] is a general-purpose tool for simulating the interaction of radiation with matter covering a wide range of applications from high-energy physics to medical and radiation physics, used by variety of organizations, including CERN and NASA[131, 132]. The code is the standard tool used at CERN for dosimetry, radioprotection and beam-machine interaction studies[117].

FLUKA reads user input from an ASCII “standard input” file which contains a variable number of settings (“options”), each consisting of one or more lines (“cards”). The typical structure of a FLUKA input file is the following:

- Titles and comments for documentation purposes.

- Geometry. FLUKA uses constructive solid geometry (CSG) which allows creating a complex surface or objecting by using Boolean operators to combine simpler objects.
- Definition of the materials.
- Material assignments.
- Detectors. Each of these is a phase space domain (region of space, particle direction and energy) where the operator wants to calculate the estimates of a physical quantity such as fluence, etc.
- Biasing.
- Additional settings such as energy cut-offs, step size, physical effects not simulated by default, particles not to be transported, etc.
- Special commands involving magnetic fields, time-dependent calculations, writing of history files, transport of optical photons, event-by-event scoring, calling user-written routines, etc.
- Initialization of the random number sequence in order to get the estimation of statistical error.
- Starting signal and number of requested histories.

Fluka has a wide set of physics interactions available which are described by detail in the manual[133]. As for our problem, it is important to know that Fluka allows semi-analogue mode of simulating radioactive decay. In this mode each single radioactive nucleus is treated in a Monte Carlo way like all other unstable particles: a random decay time, random daughters, random radiation are selected and tracked.

We'll run PRECISION physics set-up with activated detail transport of electrons, positrons and photons in addition to activated Rayleigh scattering and inelastic form factor corrections to Compton scattering and Compton profiles, detailed photoelectric edge treatment and fluorescence photons, multiple scattering, photon polarization taken into account for Compton, Rayleigh and photoelectric effects. Transport of charged particles is achieved through an original transport algorithm[134], including complete multiple Coulomb scattering treatment. At each transport step the fluctuations of energy of the discrete event and the continuous energy loss are taken into account. Accurate reproduction of average ionization and its fluctuations are performed due to a statistical approach alternative to the standard Landau and Vavilov[135]

Photoelectric effect with accurate photoelectron angular distribution is based on the fully relativistic theory of Sauter[136]. In addition, the photon polarisation is included for Compton, Rayleigh and photoelectric effects.

The lowest transport limit for electrons is 1 keV. The multiple scattering model becomes inaccurate below 20-30 keV in high Z materials, but optionally a single-scattering alternative may

be activated upon the request. It allows getting reasonable results in any material in the low energy range. As for photons, the lowest transport limit is 1 keV. But it must be noted that fluorescence emission may be misjudged at energies lower than the K-edge in high-Z materials, because of Coster-Kronig effect[133]. The minimal recommended energy for primary photons is about 5 to 10 keV.

In this project we do not limit the production but we set transport cut. Due to practical reasons and associated problems of low-energy transport a particle transport threshold is set at 100 keV by the selected default options.

Typical input file is shown in the **fig.10** below.

```
TITLE
Oras_Kapsule
GLOBAL      1000.0      0.0      0.0      0.0      1.0      0.
DEFAULTS                                          PRECISIO
BEAM                                           ISOTOPE
BEAMPOS        0.0      0.0      0.0
BEAMPOS              0.065            0.36               CYLI-VOL
HI-PROPE       77.     192.
GEOBEGIN                                          COMBNAME
   0    0              MC-CAD
SPH ASphere1   0.00 0.00 0.00 98.00
SPH ASphere2   0.00 0.00 0.00 103.00
SPH ASphere3   0.00 0.00 0.00 200.00
SPH extvoid    0.00 0.00 0.00 1000.00
SPH intvoid    0.00 0.00 0.00 500.00
RCC shell1     0.00 0.00 -0.18 0.00 0.00 0.45 0.09
RCC shell2     0.0 0.0 0.27 0.0 0.0 0.2 0.07
SPH shell3     0.00 0.00 -0.18 0.09
RCC source     0.00 0.00 -0.17 0.00 0.00 0.36 0.065
END
BLACKHOL     5 +extvoid  -intvoid
VOID         5 +intvoid  -ASphere3
AIR2         5 +ASphere3  -ASphere2
AIR3         5 +ASphere2  -ASphere1
AIR1         5 +ASphere1  -shell1  -shell2  -shell3
STEEL        5 +shell1  -source | +shell2 | +shell3  -source
IRIDIUM      5 +source
END
GEOEND
MATERIAL       77.           22.42                  IRIDIUM
MATERIAL       24.           7.18                   CHROMIUM
MATERIAL       25.           7.21                   MANGANES
MATERIAL       15.           1.82                   PHOSPHO
MATERIAL       16.           2.07                   SULFUR
* Steel316LN
* Stainless steel AISI316LN
MATERIAL                     7.8                    SS316LN
COMPOUND    -0.67145     IRON    -0.185  CHROMIUM   -0.1125    NICKELSS316LN
COMPOUND      -0.02  MANGANES     -0.01   SILICON  -0.00045   PHOSPHOSS316LN
COMPOUND     -0.0003    SULFUR   -0.0003    CARBON              SS316LN
MATERIAL       78.           21.45                  PLATINUM
* Ir192
*
MATERIAL                    21.78                   Ir192
COMPOUND       -0.3   IRIDIUM     -0.7  PLATINUM              Ir192
MATERIAL       9.          0.001696                FLUORINE
```

Setting up global values and beam properties. In our case, we choose an isotope source

Modelling the geometric primitives

Using boolean operators to establish the geometrical regions

Material and compound description

```
* 104 Air dry (near sea level)
*
MATERIAL              .00120484                    AIR
COMPOUND  -1.248E-4   CARBON -0.755267  NITROGEN -0.231781   OXYGENAIR
COMPOUND  -0.012827   ARGON                          AIR
ASSIGNMA   BLCKHOLE  BLACKHOL
ASSIGNMA    VACUUM    void
ASSIGNMA      AIR     AIR3
ASSIGNMA      AIR     AIR2
ASSIGNMA      AIR     AIR1
ASSIGNMA    SS316LN   STEEL
ASSIGNMA     Ir192   IRIDIUM
RADDECAY      2.

DCYSCORE      -1.              regdose     dose       USRBIN
DCYSCORE      -1.                energ     energ      USRTRACK
USRBIN       12.     DOSE     -30.     AIR3             regdose
USRBIN       AIR3                                &
USRBIN       11.     DOSE     -32.     200.      0.0     50.dose
USRBIN       0.0      0.0     -50.     300.      1.     300. &
USRTRACK     -1.    ENERGY    -31.     AIR3             500.energ
USRTRACK     1E-2     1E-7                           &
SCORE       ENERGY
RANDOMIZ      1.
START        1E8
STOP
```

Assigning the materials to the regions

Activating the decay physics for the isotope source

Setting up the detectors

Initializing the random seed and setting up the number of histories

Figure 10. The example of input file used for the (1) simulation

It should be stated that FLUKA has been developed to be a tool but not a toolkit. It is built and maintained with the most accurate physical models utilizing so called microscopic approach which gives the optimized performance at the single interaction level. Referring to Batisttoni[137], "[...] microscopic approach preserves correlations within interactions and among the shower components, and it provides predictions where no experimental data are directly available". There is a great potential of the use of FLUKA to medical applications, which in addition allows to translate DICOM files into voxel geometry as part of the Boolean geometry package of FLUKA[138].

3.7 Technical equipment

The MC simulation of complex geometries require a lot of computational power as billions of the events should be modelled typically to achieve the reasonable relative error. For such projects as the current one the cluster sites are need to gain results within the reasonable time frame.

For this project the services of High Performance Computing Center (HPCC) of the Lithuanian National Center of Physical and Technology Sciences (NCPTS) at Physics Faculty of Vilnius University („HPC Saulėtekis")[139] has been used. The 128-core cluster site has been assigned for the needs of the simulations in this work which. The total amount of calculations time used for the all the simulations including the testing is estimated approx. 800 hr. As for the comparison, the job with the supercomputing facility took a little bit over 30 days when a typical desktop PC with 4-core pc will took more than 3 years of continuous run. This can be seen as

illustration of the computational needs for MC simulations.

The cluster consists of 16 calculation nodes. Each node has double Intel Xeon E5335 CPU resulting in 8-core computational power, 20-32GB RAM, 250GB 7.2K HDD. The nodes are connected through 1 Gbps network.

3.8 Evaluation of uncertainties

It is necessary to calculate the dose-rate constant accurately in order to obtain the absolute dose rates from the given air-kerma strength of the sources. Monte Carlo simulations can avoid such experimental uncertainties resulting from detector positioning and response artifacts and can yield artifact-free dose-rate estimates at the various distances[1]. However, the accuracy of Monte Carlo is limited by the effects of geometric uncertainty, internal component movement, tolerances in the fabrication of sources, and small manufacturing changes on the uncertainty of calculated dose-rate distributions. In addition, it can be affected by inaccuracies in the geometric configuration of the source, uncertainties in the cross-sections and the modeling of the physical processes in the Monte Carlo code.

In general, the type B systematic uncertainty in MC simulations of radiation transport is influenced by used physics models, assumed transport assumptions, imperfect algorithms, input data uncertainty, the actual material composition, geometrical uncertainty, etc. In addition, there can be mistakes in the code or user mistakes such as mistyping the inputs, wrong normalization, etc. Type B uncertainties have not been systematically addressed in this work. A detailed discussion for their estimation and the difficulties associated with this question can be found in TG-43 associated reports presented in the first parts of the thesis. However, some remarks and notes are given for every simulation results if relevant.

Type A type uncertainty estimates are obtained as standard deviations of repeated measurement results. FLUKA code calculates the statistical error from for batches of several histories. The standard deviation of an estimator calculated from batches or from single histories is an estimate of the standard deviation of the actual distribution ("error of the mean" or "statistical error"). It is recommended to run at least 5-10 batches of comparable size[133]. The MCNP guideline[140–142] gives an insight of estimating the statistical error (**table 2**) , which is confirmed as working with other codes[133]. It must be noted, however, that it is empirically based on experience, not on a mathematical proof.

In this work we treat type A uncertainties with in-built tools in Flair tool and providing the statistical error value for every simulation in the results. Due to available technical resources we are able to keep it low.

Table 2. Estimation of relative error

Relative error	Quality of Tally
50 to 100%	Garbage
20 to 50%	Factor of a few
10 to 20 %	Questionable
< 10%	Reliable (except for detectors)
< 5%	Reliable

.

There are certain methodology requirements to be implemented into Monte Carlo modeling for testing and referencing the dose-rate estimates for the clinical use[1, 130]. It must be stated, however, that the purpose of this thesis is not to provide a ready-to-use clinical reference but rather give insights on the possible heterogeneities due to different tissues, therefore not all the requirements are followed-up as they should not influence the overall result we are intend to achieve.

4. SIMULATIONS AND RESULTS

4.1 Introduction. Global parameters

We have used FLUKA version 2011.2c.5[118] with following supporting software Flair[143] and SimpleGeo[144].

The modeled encapsulated source (**fig.11**) has an active core made of ^{192}Ir of effective density of 22.42 g/cm3 and active length of 3.6 mm. with active diameter of 0.65 mm. It is enclosed by the stainless steel AISI316LN encapsulation of density 7.8 g/cm3 with composition of iron, chromium, manganese, silicon, phosphorus, sulfur and carbon. The capsule is attached on a stainless steel cable with a diameter of 0.7 mm with length taken into the simulation not more than 2 mm.

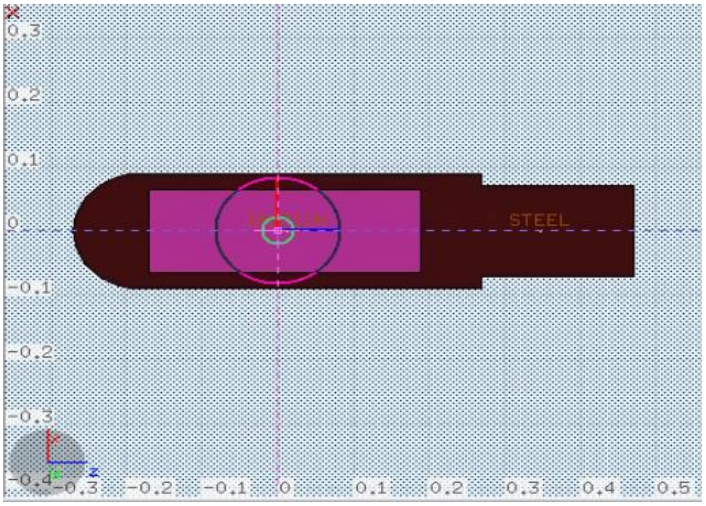

Figure 11. The modelled geometry for encapsulated source

The following simulations were run:

(1) the encapsulated ^{192}Ir source in the 30 cm radius sphere when medium is the air and when the medium is the water for comparison purpose;

(2) the non-encapsulated ^{192}Ir source (an active core only) in the water sphere of 30 cm radius versus the encapsulated source in the water sphere of the diameter for the comparison purpose;

(3) the non-encapsulated ^{192}Ir source inserted in the tongue region of anthropomorphic human head phantom, two stages: a) with all regions equivalent to the water; b) with all regions modelled to the tissue-equivalent.

The exact input files of 1-3 models are listed accordingly in the appendices A-E.

4.2 Simulation I. The encapsulated source in the air and water sphere

The purpose of the simulation is to get an initial reference data and compare it with dose absorption in the water medium. In the first simulation the encapsulated source were placed in the 150 cm radius sphere with the medium equivalent to dry air, and after that the simulation we re-run with medium switched to the water. The simulation is run in 10 batches each with 10E9 histories reaching 10E10 histories in all. The radial dose rate decrease is shown in the graphs below per primary particle **(fig. 11-12)**.

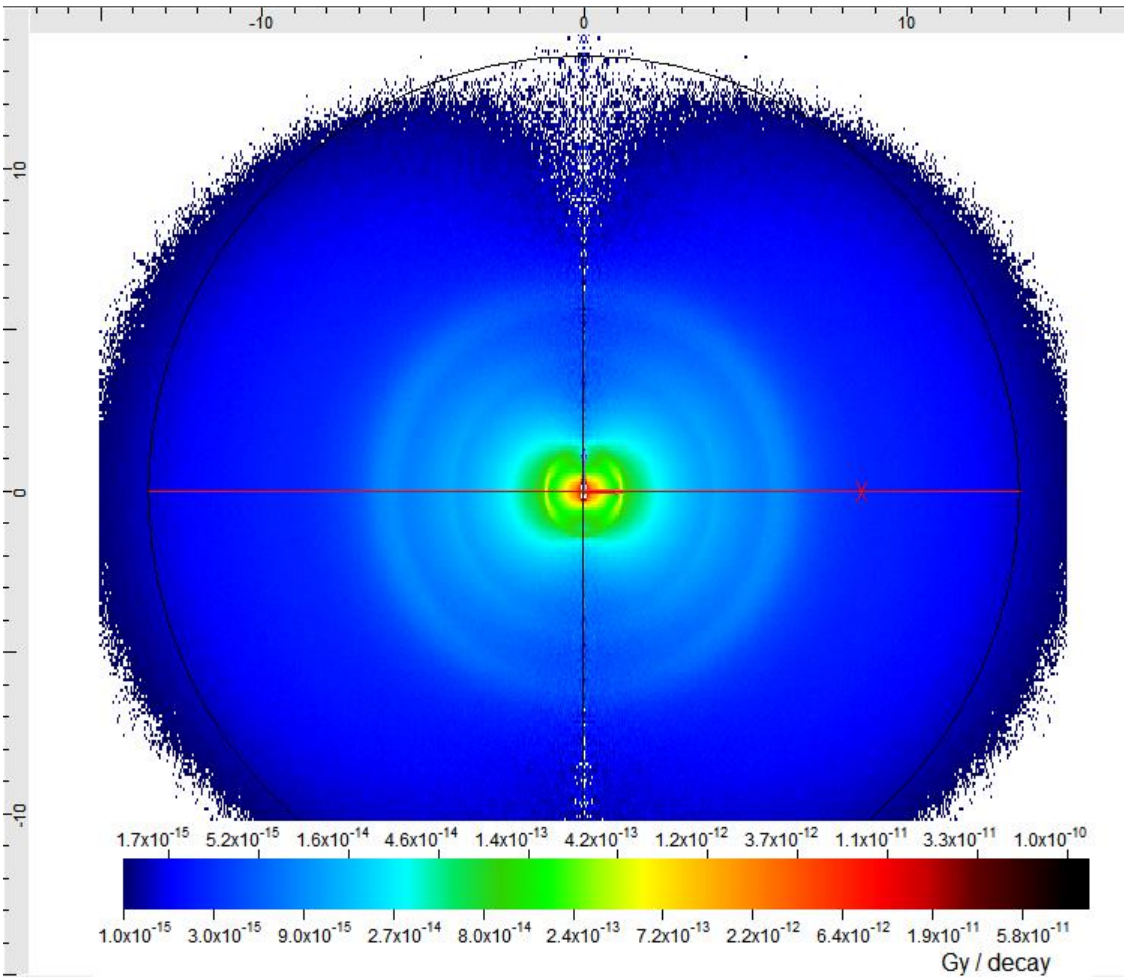

Figure 12. Z-X plane of dose distribution in the air sphere

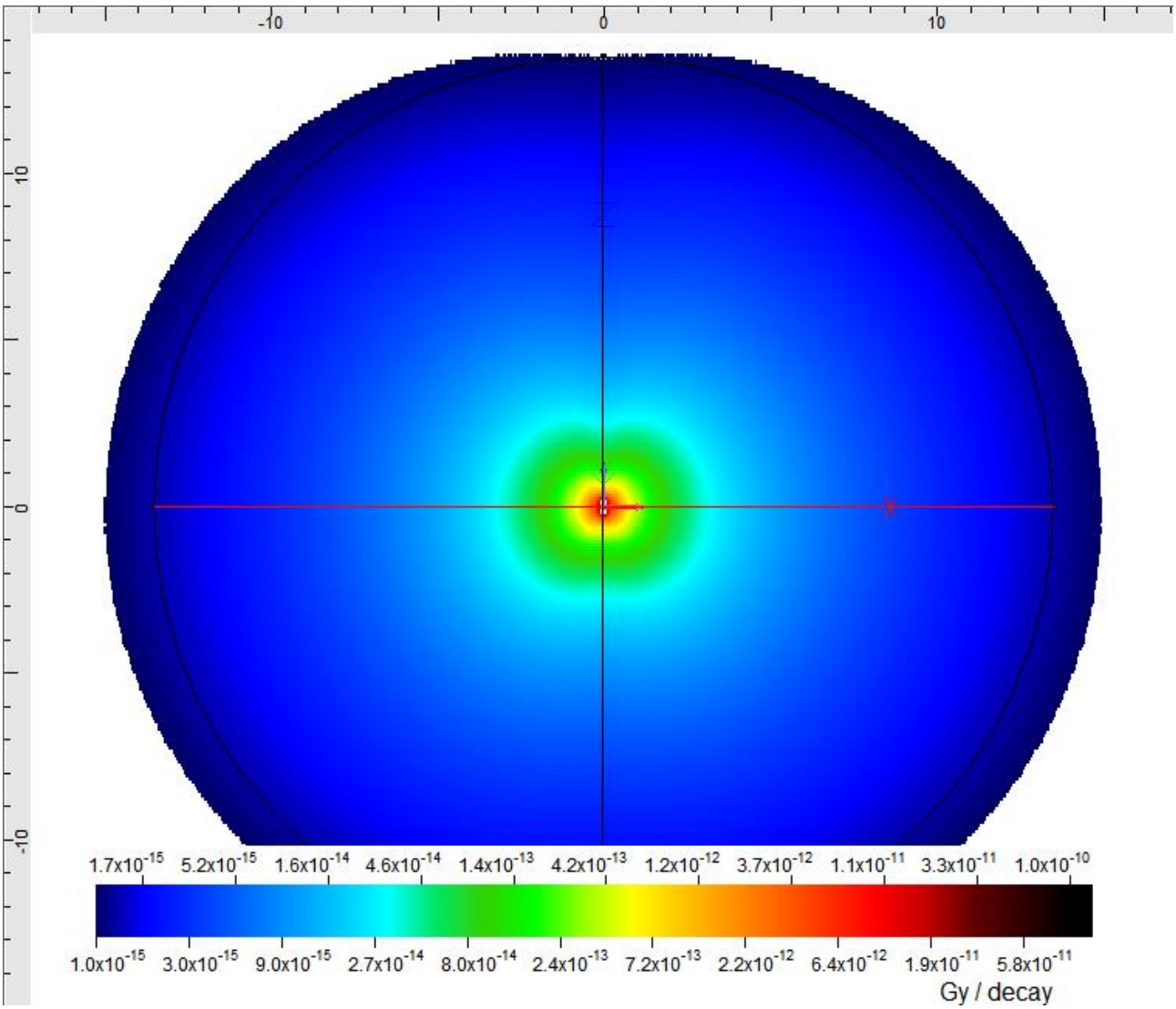

Figure 13. Z-X plane of dose distribution in the water sphere

In the graphs (**fig. 12-13**) the dose per decay is compared in the air and water mediums. The relative error is kept below 15% in the distance up to 30 cm. The graphs below are showing the dose distribution per decay in the relevant distances for the brachytherapy (radius up to 15 cm).

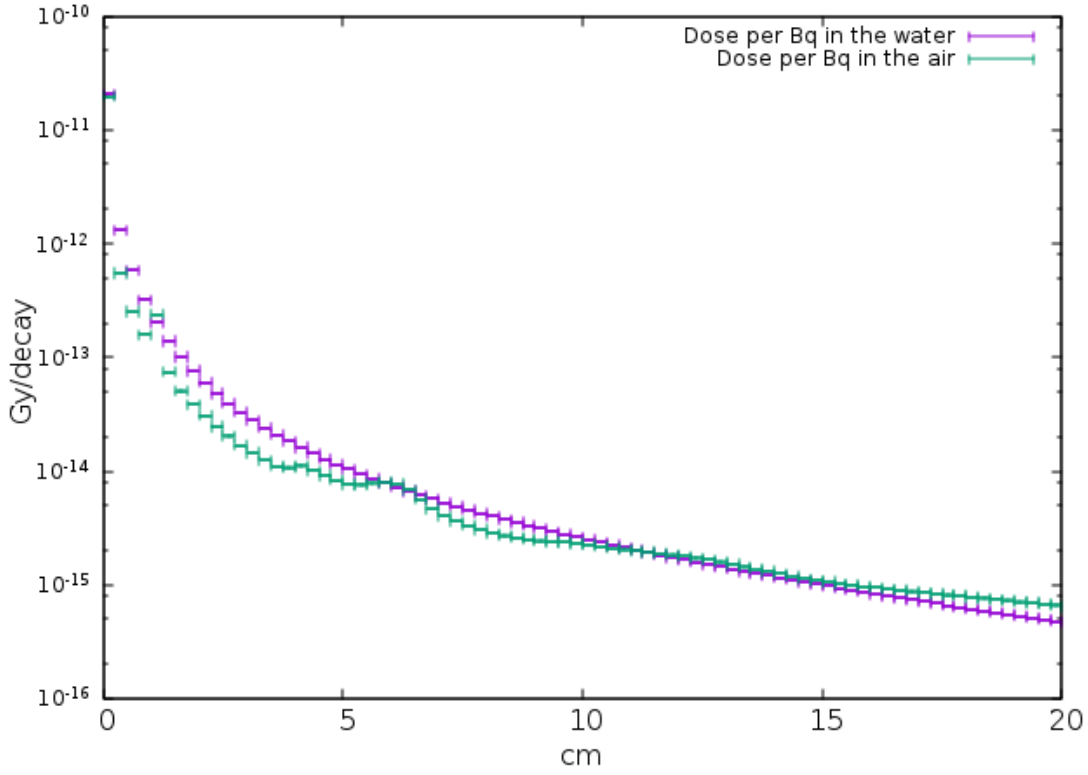

Figure 14. Dose per decay comparison in the air and water medium up to 20 cm from the active core center

The energy spectra graph was produced. As expected, the main energy range is 0.136-1.06 MeV range (**fig.15**). It is comparable with other works that report the similar energy spectra[145, 146] (**fig. 16**).

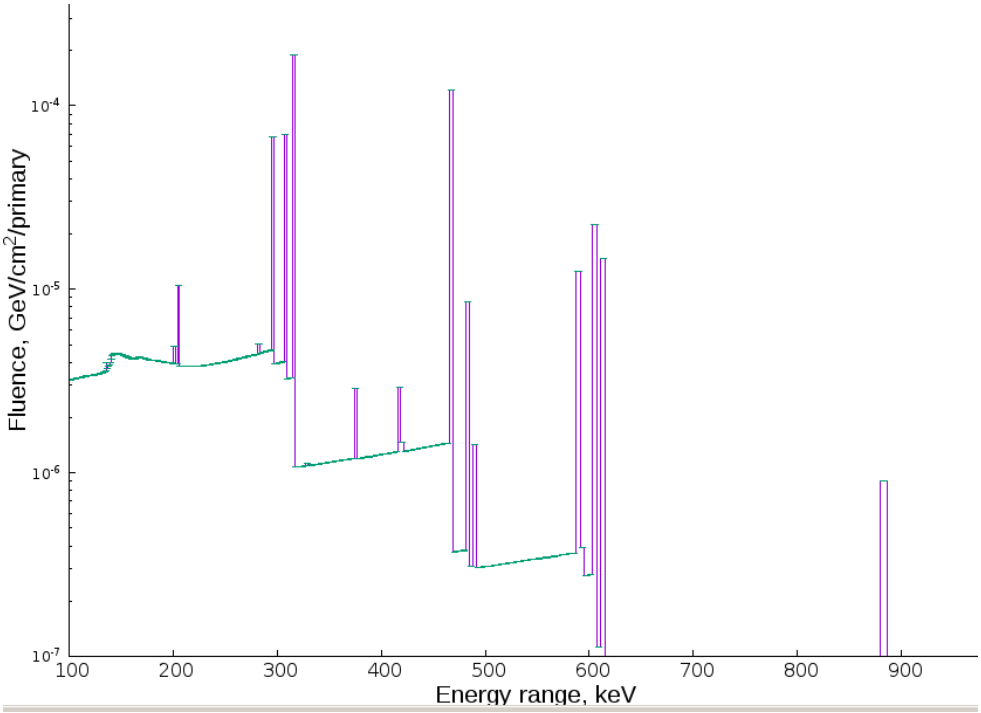

Figure 15. ^{192}Ir energy spectrum obtained in this project

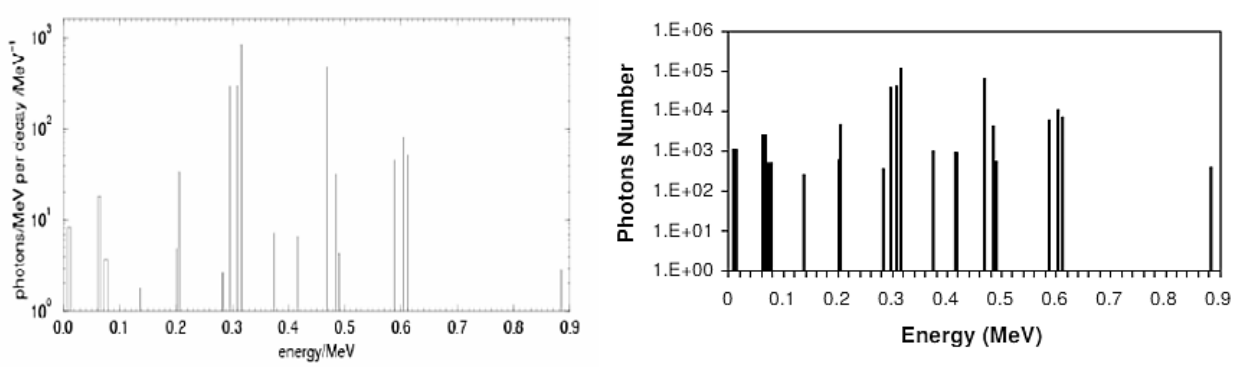

Figure 16. ^{192}Ir energy spectrum with comparison from other works: the results by Rodrigues et al[146] in the left graph and the results by Borg et al[145] in the right graph

4.3 Simulation II. The encapsulated compared with non-encapsulated source in the water sphere

It is not possible to directly combine the combinatorial geometry with voxel geometry while setting the modeling environment. As our main simulation will proceed in the voxelized human phantom, it means that we cannot model the encapsulated source inside. Instead the appropriate volume inside the phantom will be equalized to the size and parameters of the active core only. In such way it is meaningful to run the simple simulation to determine the possible differences between the dose distributions of encapsulated source versus active core only. The simulation was run in 10 batches with 10^8 histories each resulting in 10^9 histories and <5% relative error. The **fig.17** below shows that there is no major difference in the dose per decay scoring in the water medium in both cases. It should be noted that the capsule absorbs the beta rays created through the source decay whiles photons are mostly not affected.

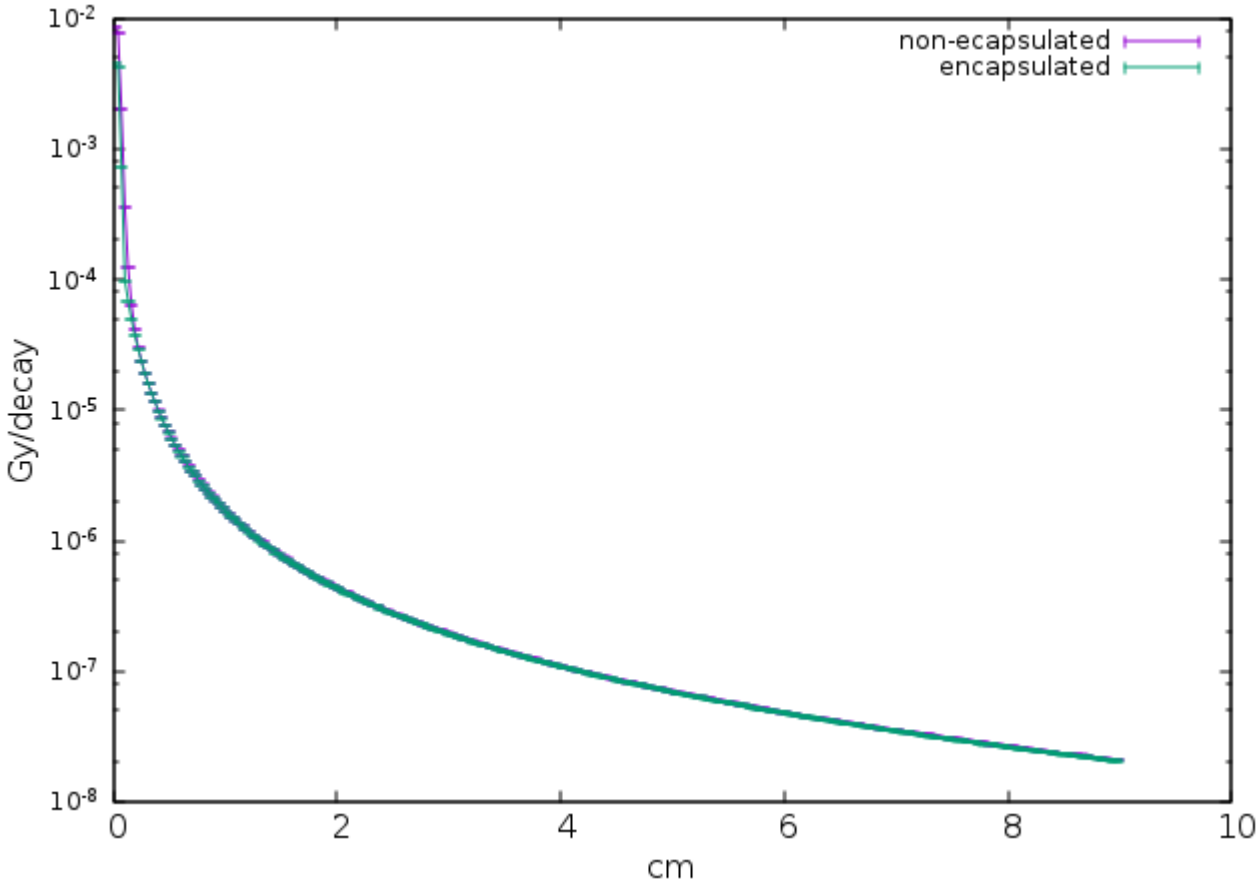

Figure 17. Comparison of encapsulated vs non-encapsulated source dose per decay

4.4 Simulation III. Dose distribution in anthropomorphic human head phantom

The used anthropomorphic human head model was adapted from Zubal phantom[2, 3, 96] in which x-ray CT was used to create a computerized 3-dimensional 128x128x243 byte volume array modeling all major internal structures of the body of size . Each voxel of the volume contains an index number designating it as belonging to a given organ or internal structure (**fig.18**).

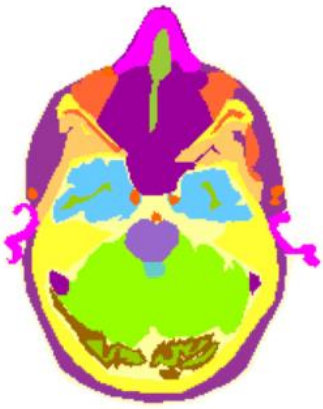

Figure 18. Sample image of Zubal head phantom[97]

For this project we investigated the head part only to which 43 slices belong thus creating

128x128x43 active volume which consists of isotropic voxel dimensions of 4 mm.

Utilizing the special FORTRAN code we have converted the available phantom data to Fluka .vxl format which serves as an input for the simulation of the radiation transport using the voxel geometry (**fig.19**). The SimpleGeo[144] auxiliary software has been used to visualize it.

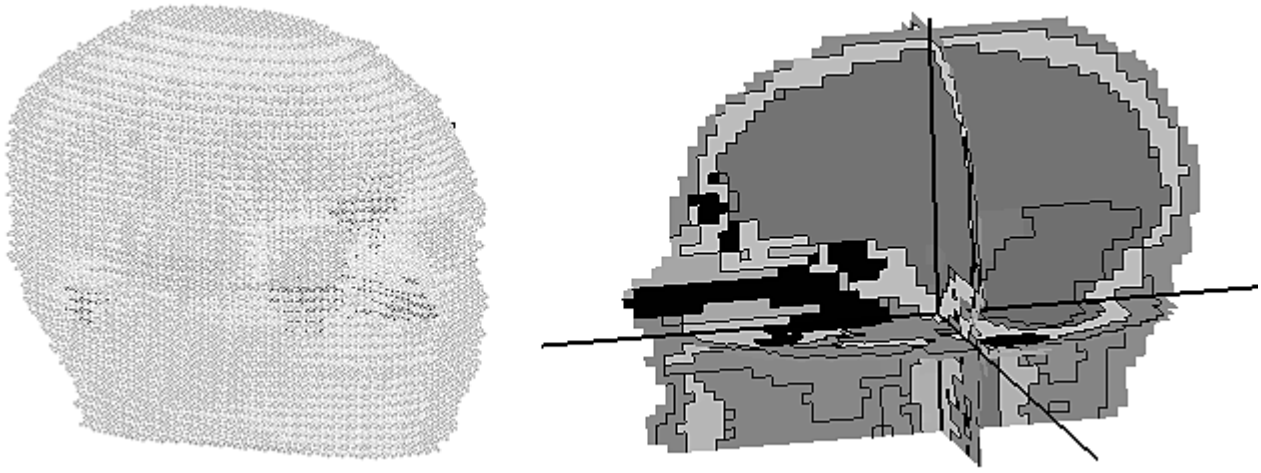

Figure 19. Zubal head phantom retransformed to the FLUKA .vxl format during the project. 3D shaded phantom is seen in the left side while the internal structure of the phantom with anatomical regions are shown in the right side

We simulated the dose distribution of ^{192}Ir source placed in the anthropomorphic head phantom region representing the middle of tongue. Two simulations were run. In the first simulation the medium of the all regions of the phantom were selected as water (i.e. *water phantom).* In the second simulation the anatomically-equivalent medium regions were created according the ICRU report and (i.e. *tissue phantom).* Each simulation was run in 100 batches containing of 10^8 histories resulting in 10^{10} histories each thus enabling to keep the relative error below 5%.

The tissue composition was taken from literature reports, specifically by ICRU report No.46[5], ICRP's phantom report[93] and work from Woodard and White[147]. All the sources are indicated in the **table 3.**

In the following **figures 20-24** the inhomogeneity of *tissue phantom* in comparison with *water phantom* can be observed, especially in the air-filled sinus region. The fluctuations may be observed in the right picture representing the dose distribution in the *tissue phantom*. The **fig. 25** shows the uncertainty regions with corresponding values of relative error of the value for that bin.

Table 3. The media of the simulation phantoms

Region	**Organ corresponding the region**	**Media of the first simulation (*water* phantom)**	**Media of the second simulation (*tissue* phantom)**
VOXEL02	skin	Water	Skin(ICRU)
VOXEL03	skeletal muscle	Water	Muscle skeletal (ICRU)
VOXEL04	jaw bone	Water	Bone, compact (ICRU)
VOXEL05	fat	Water	Adipose tissue (ICRU)
VOXEL06	pharynx	Water	Tissue, soft (ICRU)
VOXEL07	blood pool	Water	Blood (ICRU)
VOXEL08	bone marrow	Water	Skeleton-RedMarrow (Woodward, 1986)
VOXEL09	spine	Water	Bone, compact (ICRU)
VOXEL10	spinal cord	Water	Brain(ICRU)
VOXEL11	tongue	Water	Tissue, soft (ICRU)
VOXEL12	teeth	Water	Bone, compact (ICRU)
VOXEL13	spinal canal	Water	Water
VOXEL14	dens of axis	Water	Bone, compact (ICRU)
VOXEL15	hard palate	Water	Bone, compact (ICRU)
VOXEL16	skull	Water	Bone, compact (ICRU)
VOXEL17	sinuses/mouth cavity	Water	Air
VOXEL18	brain	Water	Brain(ICRU)
VOXEL19	medulla oblangata	Water	Brain(ICRU)
VOXEL20	cerebellum	Water	Brain(ICRU)
VOXEL21	cartilage	Water	Skeleton-Cartilage(Woodward, 1986)
VOXEL22	pons	Water	Brain(ICRU)
VOXEL23	eye	Water	Tissue, soft (ICRU)
VOXEL24	lens	Water	Eye lens(ICRU)
VOXEL25	optic nerve	Water	Brain(ICRU)
VOXEL26	cerebral falx	Water	Brain(ICRU)

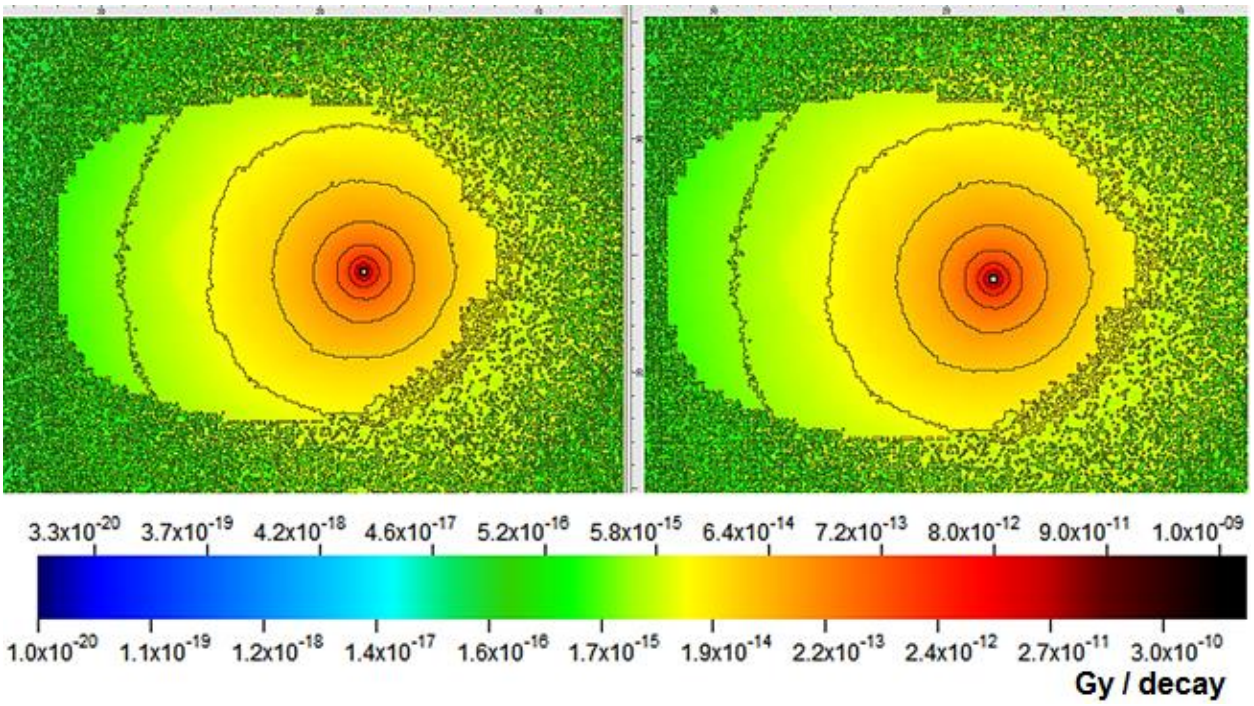

Figure 20. Dose distribution in water phantom (left) and tissue phantom (right). Transverse plane

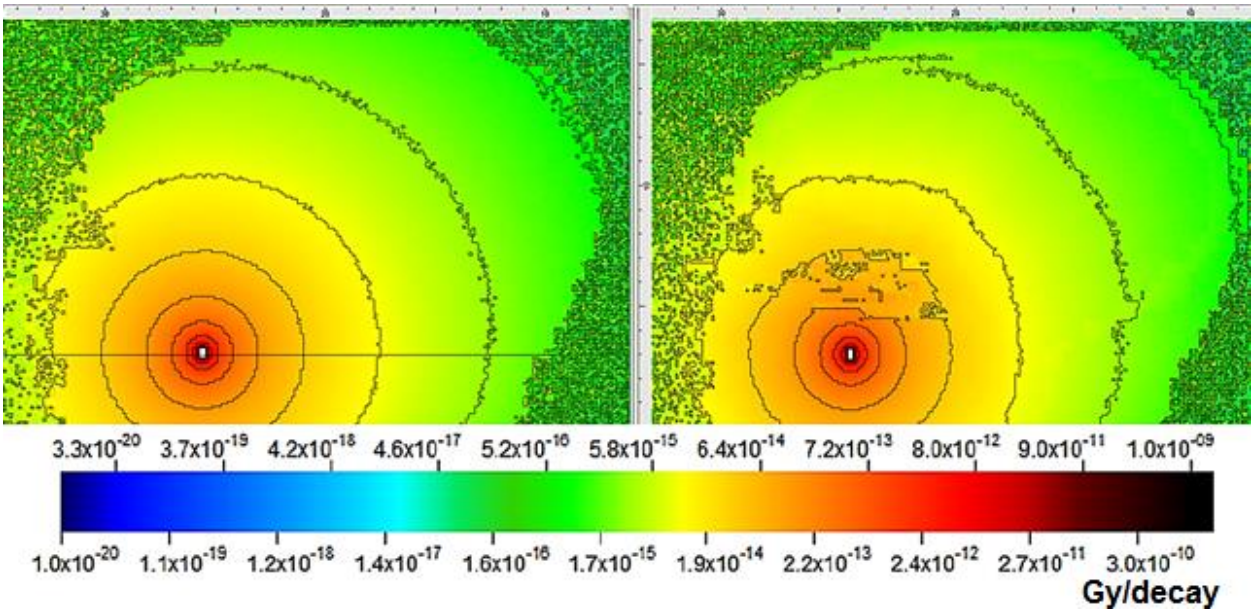

Figure 21. Dose distribution in water phantom (left) and tissue phantom (right). Sagittal plane

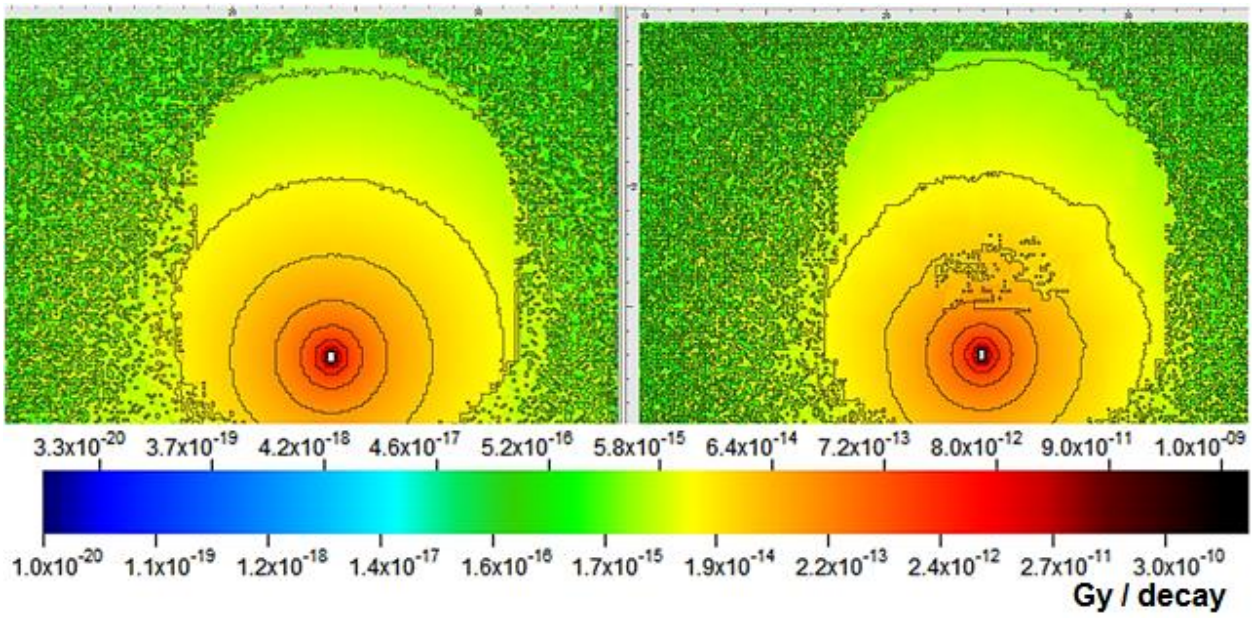

Figure 22. Dose distribution in water phantom (left) and tissue phantom (right). Coronal plane

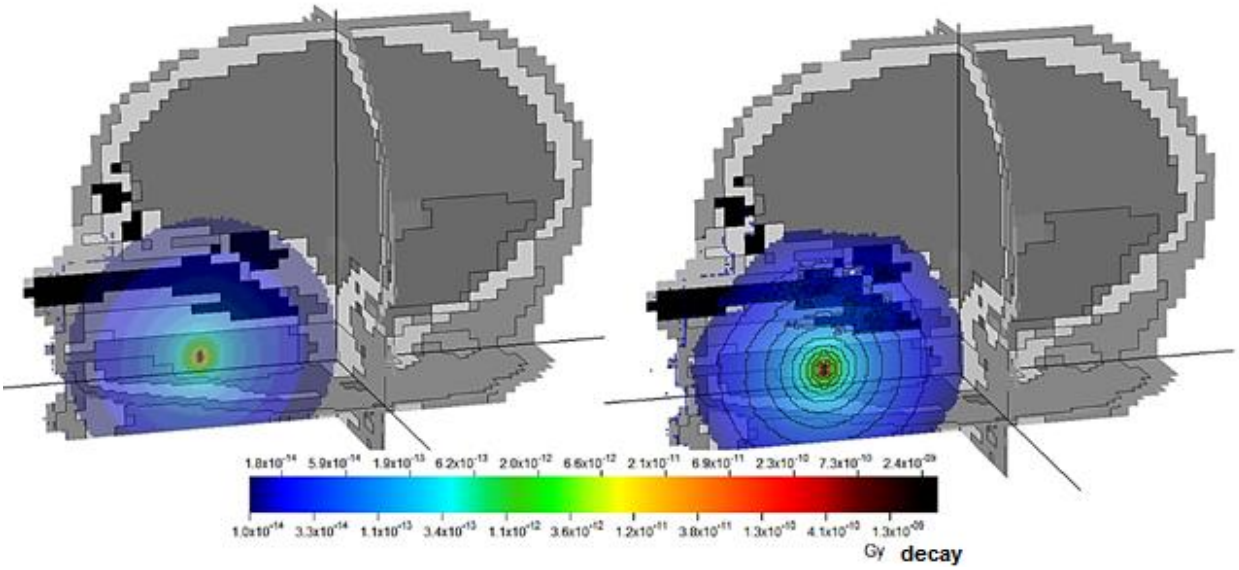

Figure 23. Dose distribution in water phantom (left) and tissue phantom (right). 3D model with dose limit to $1E^{-14}$ / Bq.

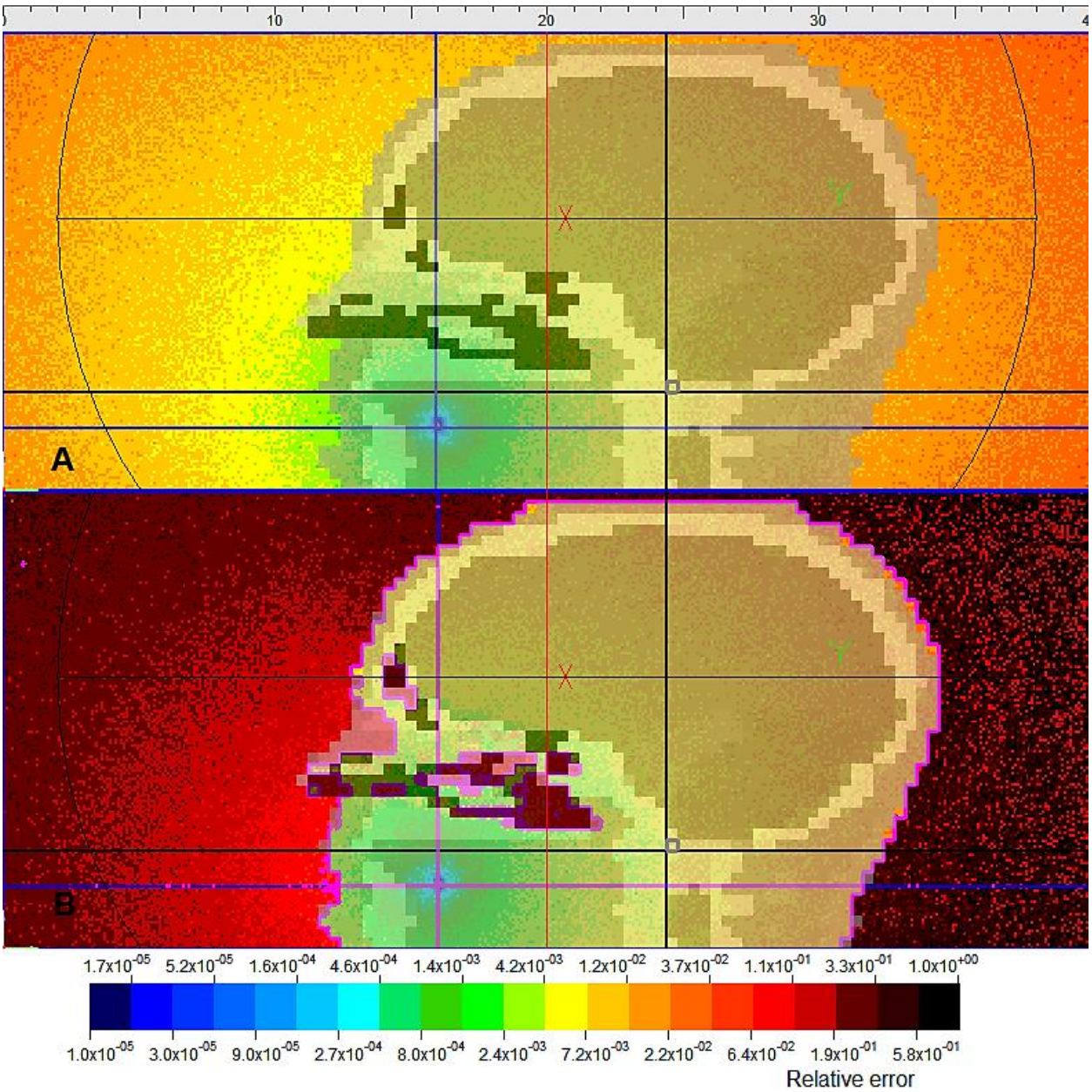

Figure 244. The value of relative error for every bin for the water phantom simulation (A) and tissue phantom (B). Note significantly higher uncertainty in the latter. Pink threshold line shows the limit of 5% relative value

The summary **table 4** and the graph (**fig. 25**) is shown below illustrating the differences in dose distribution in the various regions.

Table 4. The summary table of the phantom simulations with ^{192}Ir

Organ name	Tissue Appointed	Volume, cm^3	Dose in Gy per decay when region material is water	Dose in Gy per decay when tissue equivalent is selected	Difference
skin	Skin(ICRU)	638.592	3.696E-15	3.496E-15	-5.71%
skeletal muscle	Muscle skeletal (ICRU)	740.736	1.186E-14	1.161E-14	-2.21%
jaw bone	Bone, compact (ICRU)	75.712	2.334E-14	2.395E-14	2.52%
fat	Adipose tissue (ICRU)	31.936	7.405E-15	7.533E-15	1.70%
pharynx	Tissue, soft (ICRU)	10.56	2.236E-14	2.242E-14	0.25%
blood pool	Blood (ICRU)	15.232	6.039E-15	5.973E-15	-1.10%
bone marrow	Skeleton-RedMarrow (Woodward, 1986)	4.608	8.541E-15	8.467E-15	-0.87%
spine	Bone, compact (ICRU)	56.256	6.557E-15	6.915E-15	5.17%
spinal cord	Brain(ICRU)	9.152	5.069E-15	4.859E-15	-4.33%
tongue	Tissue, soft (ICRU)	37.632	1.109E-12	1.108E-12	-0.06%
teeth	Bone, compact (ICRU)	16.64	3.210E-14	3.309E-14	2.99%
spinal canal	Water	6.528	5.410E-15	5.035E-15	-7.44%
dens of axis	Bone, compact (ICRU)	0.96	1.035E-14	1.110E-14	6.77%
hard palate	Bone, compact (ICRU)	29.12	4.866E-14	4.890E-14	0.50%
skull	Bone, compact (ICRU)	519.296	3.580E-15	3.840E-15	6.76%
sinuses/mouth cavity	Air	82.368	1.852E-14	1.750E-14	-5.83%
brain	Brain(ICRU)	1171.136	2.862E-15	2.862E-15	0.03%
medulla oblangata	Brain(ICRU)	1.216	5.660E-15	5.327E-15	-6.24%
cerebellum	Brain(ICRU)	157.952	2.351E-15	2.190E-15	-7.38%
cartilage	Skeleton-Cartilage(Woodward, 1986)	53.76	9.228E-15	8.805E-15	-4.81%
pons	Brain(ICRU)	22.336	4.723E-15	4.716E-15	-0.16%
eye	Tissue, soft (ICRU)	15.488	7.675E-15	8.321E-15	7.76%
lens	Eye lens(ICRU)	1.472	6.105E-15	6.577E-15	7.18%
optic nerve	Brain(ICRU)	5.952	1.068E-14	1.075E-14	0.62%
cerebral falx	Brain(ICRU)	13.12	1.515E-15	1.582E-15	4.23%

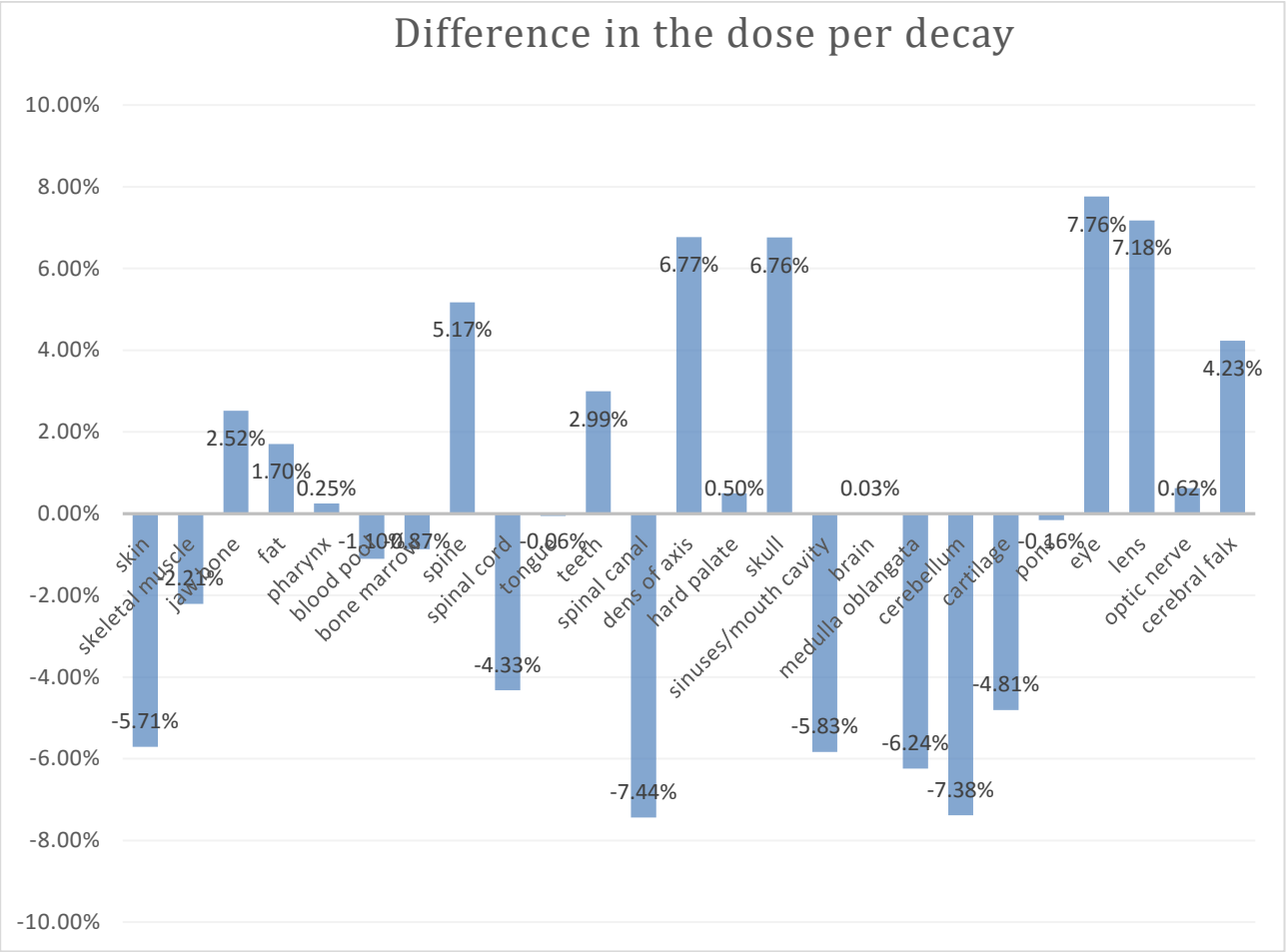

Figure 25. Differences in dose per decay between water and tissue phantom simulations with ^{192}Ir source

5. CONCLUSIONS

The simulation of the dose distribution of brachytherapy source within 3D voxelised anthropomorphic human head phantom has been performed taking into account corresponding tissue compositions. The discrepancies between the dose values obtained from homogeneous media phantom and from modified heterogeneous media phantom calculations were assessed.

1. The visualization of isodoses shows that actual dose distributions within appointed tissue equivalents differ from the clinically calculated distributions according TG-43 protocol when homogenous water medium is taken into calculations.
2. It is shown that the differences in the absorbed dose values between the water-built and tissue-built phantoms are up to 7.76 %. The dense material such as bone absorbed more energy and received higher dose then water-equivalent. The dose increase in the eye region could be result of the less energy absorption in the air-filled sinus region.
3. The data of the recognized Zubal phantom were translated to the format usable by FLUKA package. The translated phantom allows making the certain modifications in it thus giving an opportunity to use it in many other problems in the radiotherapy.
4. The project pioneered the methodic way in Lithuania of 3D tissue-based phantom use for Monte Carlo simulation of radiation transport for medical physicists. The tools used and described *know-how* can be easily re-used to solve any problem of such kind.

The project outcome confirms the impact of heterogeneous tissues to the dose distribution of brachytherapy source and enables to analyse the sensitivity of tissue composition on absorbed dose. It also may be used as the quality assurance tool for individual special-case patients such with certain implants near the source path to gain additional data next to the one provided by conventional treatment planning system.

6. ACKNOWLEDGEMENTS

I would first like to thank my thesis advisor prof. D. Adlienė of the faculty of Mathematics and Natural Sciences at Kaunas University of Technology who was always ready to help whenever I ran into a challenge or had a question about my research or writing and steered me in the right the direction whenever she thought I needed it.

I would also like to acknowledge the services of High Performance Computing Center (HPCC) of the Lithuanian National Center of Physical and Technology Sciences (NCPTS) at Physics Faculty of Vilnius University („HPC Saulėtekis“) which provided with technical basis to perform the simulations of this project.

7. BIBLIOGRAPHY

1. RIVARD, Mark J, COURSEY, Bert M, DEWERD, Larry a, HANSON, William F, HUQ, M Saiful, IBBOTT, Geoffrey S, MITCH, Michael G, NATH, Ravinder and WILLIAMSON, Jeffrey F. Update of AAPM Task Group No. 43 Report: A revised AAPM protocol for brachytherapy dose calculations. *Medical physics* [online]. 2004. Vol. 31, no. 3, p. 633–674. [Accessed 18 March 2017]. DOI 10.1118/1.1905824. Available from: http://www.teambest.com/besttotalsolutions/PDFs/TG43_update_Iodine_Rivard_Coursey_DeWerd_et_al_March2004.pdf
2. ZUBAL, G., GINDI, G., LEE, M., HARRELL, C. and SMITH, E. High resolution anthropomorphic phantom for Monte Carlo analysis of internal radiation sources. In : *[1990] Proceedings. Third Annual IEEE Symposium on Computer-Based Medical Systems* [online]. IEEE Comput. Soc. Press, p. 540–547. [Accessed 18 March 2017]. ISBN 0-8186-9040-2. Available from: http://ieeexplore.ieee.org/document/109445/
3. ZUBAL, I. George, HARRELL, Charles R., SMITH, Eileen O., RATTNER, Zachary, GINDI, Gene and HOFFER, Paul B. Computerized three-dimensional segmented human anatomy. *Medical Physics* [online]. February 1994. Vol. 21, no. 2, p. 299–302. [Accessed 18 March 2017]. DOI 10.1118/1.597290. Available from: http://www.ncbi.nlm.nih.gov/pubmed/8177164
4. WHITE, D. R., BOOZ, J., GRIFFITH, R. V., SPOKAS, J. J. and WILSON, I. J. ICRU Report 44: Tissue Substitutes in Radiation Dosimetry and Measurement. *Journal of the ICRU* [online]. 1989. Vol. os23, no. 1. DOI 10.1093/jicru/os23.1.Report44. Available from: http://www.icru.org/home/reports/photon-electron-proton-and-neutron-interaction-data-for-body-tissues-report-46
5. INTERNATIONAL COMMISSION ON RADIATION UNITS AND MEASUREMENT. *ICRU Report 46: Photon, electron, proton and neutron interaction data for body tissues* [online]. 1992. Available from: http://www.icru.org/home/reports/photon-electron-proton-and-neutron-interaction-data-for-body-tissues-report-46
6. FERRARI, A, SALA, P R, FASSO, A and RANFT, J. FLUKA: A Multi-Particle Transport Code. . 2005.
7. BÖHLEN, T. T., CERUTTI, F., CHIN, M. P W, FASSÒ, A., FERRARI, A., ORTEGA, P. G., MAIRANI, A., SALA, P. R., SMIRNOV, G. and VLACHOUDIS, V. The FLUKA Code: Developments and challenges for high energy and medical applications. *Nuclear Data Sheets* [online]. June 2014. Vol. 120, p. 211–214. [Accessed 23 June 2016]. DOI 10.1016/j.nds.2014.07.049. Available from: http://linkinghub.elsevier.com/retrieve/pii/S0090375214005018
8. NATH, R, ANDERSON, L L, LUXTON, G, WEAVER, K a, WILLIAMSON, J F and MEIGOONI, a S. Dosimetry of interstitial brachytherapy sources: recommendations of the AAPM Radiation Therapy Committee Task Group No. 43. American Association of Physicists in Medicine. *Medical physics* [online]. 1995. Vol. 22, no. 2, p. 209–234. [Accessed 18 March 2017]. DOI 10.1118/1.597458. Available from: https://www.aapm.org/pubs/reports/rpt_51.pdf
9. AWAN, S. B., HUSSAIN, M., DINI, S. A. and MEIGOONI, A. S. Historical review of interstitial prostate brachytherapy. *Iranian Journal of Radiation Research* [online]. 2008. Vol. 5, no. 4, p. 153–168. [Accessed 27 April 2017]. Available from: http://en.journals.sid.ir/ViewPaper.aspx?ID=112670
10. LAWRENCE, DC, SONDHAUS, CA, FEDER, B and SCALLON, J. Soft X-Ray “Seeds” for Cancer Therapy 1. *Radiology* [online]. 1966. [Accessed 27 April 2017]. Available from:

http://pubs.rsna.org/doi/pdf/10.1148/86.1.143a

11. LOFTUS, TP. Standardization of cesium-137 gamma-ray sources in terms of exposure units (roentgens). *J. Res. Natl. Bur. Stand., Sect. A* [online]. 1970. [Accessed 27 April 2017]. Available from: http://nvlpubs.nist.gov/nistpubs/jres/74A/jresv74An1p1_A1b.pdf
12. LOFTUS, TP. Standardization of iridium-192 gamma-ray sources in terms of exposure. *J. Res. Nat. Bur. Stand* [online]. 1980. [Accessed 27 April 2017]. Available from: http://nvlpubs.nist.gov/nistpubs/jres/85/jresv85n1p19_A1b.pdf
13. ANDERSON, LL. Interstitial brachytherapy: physical, biological, and clinical considerations. . 1990.
14. MEISBERGER, L L, KELLER, Ronald J and SHALEK, R J. The effective attenuation in water of the gamma rays of gold 198, iridium 192, cesium 137, radium 226, and cobalt 60. *Radiology* [online]. May 1968. Vol. 90, no. 5, p. 953–7. [Accessed 16 April 2017]. DOI 10.1148/90.5.953. Available from: http://www.ncbi.nlm.nih.gov/pubmed/5643598
15. DALE, R G. Some theoretical derivations relating to the tissue dosimetry of brachytherapy nuclides, with particular reference to iodine-125. *Medical physics* [online]. March 1982. Vol. 10, no. 2, p. 176–83. [Accessed 16 April 2017]. DOI 10.1118/1.595297. Available from: http://www.ncbi.nlm.nih.gov/pubmed/6865856
16. BURNS, G S and RAESIDE, D E. Two-dimensional dose distribution around a commercial 125I seed. *Medical physics* [online]. January 1988. Vol. 15, no. 1, p. 56–60. [Accessed 16 April 2017]. DOI 10.1118/1.596151. Available from: http://www.ncbi.nlm.nih.gov/pubmed/3352551
17. WILLIAMSON, J F. Comparison of measured and calculated dose rates in water near I-125 and Ir-192 seeds. *Medical physics* [online]. July 1991. Vol. 18, no. 4, p. 776–786. [Accessed 16 April 2017]. DOI 10.1118/1.596631. Available from: http://www.ncbi.nlm.nih.gov/pubmed/1921887
18. WILLIAMSON, J F, PERERA, H, LI, Z and LUTZ, W R. Comparison of calculated and measured heterogeneity correction factors for 125I, 137Cs, and 192Ir brachytherapy sources near localized heterogeneities. *Medical physics* [online]. January 1993. Vol. 20, no. 1, p. 209–222. [Accessed 16 April 2017]. DOI 10.1118/1.597088. Available from: http://www.ncbi.nlm.nih.gov/pubmed/8455503
19. FIPPEL, M. Basics of Monte Carlo Simulations. *Monte Carlo Techniques in Radiation Therapy* [online]. 2013. [Accessed 16 April 2017]. Available from: https://www.google.com/books?hl=en&lr=&id=rGc879Q1haUC&oi=fnd&pg=PA17&dq=Matthias+Fippel+basics+of+monte+carlo&ots=ErPMwhu8Jc&sig=zjd7khejvvjSLpwHAZTLsF-kQyU
20. DEMARCO, John. Monte Carlo Techniques in Radiation Therapy. Imaging in Medical Diagnosis and Therapy. *Medical Physics* [online]. 28 May 2015. Vol. 42, no. 6, p. 3089–3089. [Accessed 16 April 2017]. DOI 10.1118/1.4919679. Available from: http://doi.wiley.com/10.1118/1.4919679
21. SECO, Joao and VERHAEGEN, Frank. *Monte Carlo Techniques in Radiation Therapy*. CRC/Taylor & Francis, 2013. ISBN 9781439804360.
22. LANDRY, Guillaume, RIVARD, Mark J, WILLIAMSON, Jeffrey F and VERHAEGEN, Frank. Monte Carlo Methods and Applications for Brachytherapy Dosimetry and Treatment Planning. *Monte Carlo Techniques in Radiation Therapy* [online]. 2013. P. 19. [Accessed 16 April 2017]. Available from: https://www.google.com/books?hl=en&lr=&id=CDnSBQAAQBAJ&oi=fnd&pg=PA125&dq=landry+Monte+Carlo+Methods+and+Applications+for+Brachytherapy+Dosimetry+and+Treatment+Planning&ots=XjN22jW3Fz&sig=KWONwolr63L5KJAtR09pxok_QrU

23. WILLIAMSON, J. F. and RIVARD, M. J. Quantitative dosimetry methods for brachytherapy. *Brachytherapy Physics, 2nd ed.* 2005. P. 233–294.
24. BRUALLA, L, RODRIGUEZ, M and LALLENA, AM. Monte Carlo systems used for treatment planning and dose verification. *Strahlentherapie und Onkologie* [online]. 2016. [Accessed 1 May 2017]. Available from: http://link.springer.com/article/10.1007/s00066-016-1075-8
25. MEIGOONI, AS, MELI, JA and NATH, R. Interseed effects on dose for 125I brachytherapy implants. *Medical physics* [online]. 1992. [Accessed 19 April 2017]. Available from: http://onlinelibrary.wiley.com/doi/10.1118/1.596871/full
26. CHIBANI, O, WILLIAMSON, JF and TODOR, D. Dosimetric effects of seed anisotropy and interseed attenuation for Pd103 and I125 prostate implants. *Medical physics* [online]. 2005. [Accessed 19 April 2017]. Available from: http://onlinelibrary.wiley.com/doi/10.1118/1.1897466/full
27. CARRIER, JF, BEAULIEU, L and THERRIAULT- PROULX, F. Impact of interseed attenuation and tissue composition for permanent prostate implants. *Medical* [online]. 2006. [Accessed 19 April 2017]. Available from: http://onlinelibrary.wiley.com/doi/10.1118/1.2168295/full
28. AFSHARPOUR, H, PIGNOL, JP and KELLER, B. Influence of breast composition and interseed attenuation in dose calculations for post-implant assessment of permanent breast 103Pd seed implant. *Physics in medicine* [online]. 2010. [Accessed 19 April 2017]. Available from: http://iopscience.iop.org/article/10.1088/0031-9155/55/16/S09/meta
29. RIVARD, Mark J., MELHUS, Christopher S., GRANERO, Domingo, PEREZ-CALATAYUD, Jose and BALLESTER, Facundo. An approach to using conventional brachytherapy software for clinical treatment planning of complex, Monte Carlo-based brachytherapy dose distributionsa). *Medical Physics* [online]. 5 May 2009. Vol. 36, no. 6, p. 1968–1975. [Accessed 1 May 2017]. DOI 10.1118/1.3121510. Available from: http://doi.wiley.com/10.1118/1.3121510
30. YEGIN, G. and SARIAYDIN, S. TPSDose43: A new TG-43 based dose calculation code for brachytherapy. *Physica Medica* [online]. 2016. Vol. 32, p. 228–229. [Accessed 1 May 2017]. DOI 10.1016/j.ejmp.2016.07.470. Available from: http://www.sciencedirect.com/science/article/pii/S1120179716306032
31. HUESO-GONZÁLEZ, Fernando, BALLESTER, Facundo, PEREZ-CALATAYUD, Jose, SIEBERT, Frank-André and VIJANDE, Javier. Towards clinical application of RayStretch for heterogeneity corrections in {LDR} permanent 125I prostate brachytherapy. *Brachytherapy* [online]. 2017. [Accessed 1 May 2017]. DOI http://doi.org/10.1016/j.brachy.2017.02.005. Available from: http://www.sciencedirect.com/science/article/pii/S1538472117300429
32. CHAMBERLAND, Marc J P, TAYLOR, Randle E P, ROGERS, D W O and THOMSON, Rowan M. egs_brachy: a versatile and fast Monte Carlo code for brachytherapy. *Physics in Medicine and Biology* [online]. 7 December 2016. Vol. 61, no. 23, p. 8214–8231. [Accessed 1 May 2017]. DOI 10.1088/0031-9155/61/23/8214. Available from: http://stacks.iop.org/0031-9155/61/i=23/a=8214?key=crossref.c79d44b1849f6121bd88590003b74a36
33. TIAN, Z., ZHANG, M., HRYCUSHKO, B., ALBUQUERQUE, K., JIANG, S. B. and JIA, X. Monte Carlo dose calculations for high-dose-rate brachytherapy using GPU-accelerated processing. *Brachytherapy* [online]. 2016. Vol. 15, no. 3, p. 387–398. [Accessed 1 May 2017]. DOI 10.1016/j.brachy.2016.01.006. Available from: http://www.sciencedirect.com/science/article/pii/S1538472116000167
34. CHIBANI, Omar and WILLIAMSON, Jeffrey F. MCPI©: A sub-minute Monte Carlo dose calculation

engine for prostate implants. *Medical Physics* [online]. 17 November 2005. Vol. 32, no. 12, p. 3688–3698. [Accessed 1 May 2017]. DOI 10.1118/1.2126822. Available from: http://doi.wiley.com/10.1118/1.2126822

35. YEGIN, G, TAYLOR, R and ROGERS, D. SU-FF-T-113: BrachyDose: A New Fast Monte Carlo Code for Brachytherapy Calculations. *Medical Physics* [online]. 2006. Vol. 33, no. 6, p. 2074. [Accessed 1 May 2017]. DOI 10.1118/1.2241038. Available from: https://www.researchgate.net/profile/Gultekin_Yegin/publication/305279948_BrachyDose_A_New_Fast_Monte_Carlo_Code_for_Brachytherapy_Calculations/data/57866bf508ae36ad40a69216/Gyegin-BrachyDose-AAPM-48-final-dr-TOPRINT.pdf
36. KAWRAKOW, I and ROGERS, D W O. The EGSnrc Code System:Monte Carlo Simulation of Electron and Photon Transport. *NRCC Report PIRS-701* [online]. 2003. [Accessed 1 May 2017]. Available from: http://nrc-cnrc.github.io/EGSnrc/doc/pirs701-egsnrc.pdf
37. YEGIN, Gultekin. A new approach to geometry modeling for Monte Carlo particle transport: An application to the EGS code system. *Nuclear Instruments and Methods in Physics Research Section B: Beam Interactions with Materials and Atoms* [online]. 2003. Vol. 211, no. 3, p. 331–338. [Accessed 1 May 2017]. DOI 10.1016/S0168-583X(03)01318-1. Available from: http://www.sciencedirect.com/science/article/pii/S0168583X03013181
38. THOMSON, RM, YEGIN, G, TAYLOR, REP, SUTHERLAND, JGH and ROGERS, DWO. Fast Monte Carlo Dose Calculations for Brachytherapy with BrachyDose. *Medical Physics* [online]. July 2010. Vol. 37, no. 7, p. 3910. [Accessed 1 May 2017]. DOI 10.1118/1.3476217. Available from: http://scitation.aip.org/content/aapm/journal/medphys/37/7/10.1118/1.3476217
39. TAYLOR, R. E. P., YEGIN, G. and ROGERS, D. W. O. Benchmarking BrachyDose: Voxel based EGSnrc Monte Carlo calculations of TG-43 dosimetry parameters. *Medical Physics* [online]. 10 January 2007. Vol. 34, no. 2, p. 445–457. [Accessed 1 May 2017]. DOI 10.1118/1.2400843. Available from: http://www.ncbi.nlm.nih.gov/pubmed/17388160
40. SUTHERLAND, J G H, FURUTANI, K M and THOMSON, R M. A Monte Carlo investigation of lung brachytherapy treatment planning. *Physics in Medicine and Biology* [online]. 21 July 2013. Vol. 58, no. 14, p. 4763–4780. [Accessed 1 May 2017]. DOI 10.1088/0031-9155/58/14/4763. Available from: http://stacks.iop.org/0031-9155/58/i=14/a=4763?key=crossref.f2eefa453aab40cb953f115783f6bec1
41. AFSHARPOUR, H, LANDRY, G, D'AMOURS, M, ENGER, S, RENIERS, B, POON, E, CARRIER, J-F, VERHAEGEN, F and BEAULIEU, L. ALGEBRA: ALgorithm for the heterogeneous dosimetry based on GEANT4 for BRAchytherapy. *Physics in Medicine and Biology* [online]. 7 June 2012. Vol. 57, no. 11, p. 3273–3280. [Accessed 1 May 2017]. DOI 10.1088/0031-9155/57/11/3273. Available from: http://stacks.iop.org/0031-9155/57/i=11/a=3273?key=crossref.141337ef984ffb23364a6795bd6b345f
42. AGOSTINELLI, S., ALLISON, J., AMAKO, K., APOSTOLAKIS, J., ARAUJO, H., ARCE, P., ASAI, M., AXEN, D., BANERJEE, S., BARRAND, G., BEHNER, F., BELLAGAMBA, L., BOUDREAU, J., BROGLIA, L., BRUNENGO, A., BURKHARDT, H., CHAUVIE, S., CHUMA, J., CHYTRACEK, R., COOPERMAN, G., COSMO, G., DEGTYARENKO, P., DELL'ACQUA, A., DEPAOLA, G., DIETRICH, D., ENAMI, R., FELICIELLO, A., FERGUSON, C., FESEFELDT, H., FOLGER, G., FOPPIANO, F., FORTI, A., GARELLI, S., GIANI, S., GIANNITRAPANI, R., GIBIN, D., GOMEZ CADENAS, J. J., GONZALEZ, I., GRACIA ABRIL, G., GREENIAUS, G., GREINER, W., GRICHINE, V., GROSSHEIM, A., GUATELLI, S., GUMPLINGER, P., HAMATSU, R., HASHIMOTO, K., HASUI, H., HEIKKINEN, A., HOWARD, A., IVANCHENKO, V., JOHNSON, A., JONES, F. W., KALLENBACH, J., KANAYA,

N., KAWABATA, M., KAWABATA, Y., KAWAGUTI, M., KELNER, S., KENT, P., KIMURA, A., KODAMA, T., KOKOULIN, R., KOSSOV, M., KURASHIGE, H., LAMANNA, E., LAMPEN, T., LARA, V., LEFEBURE, V., LEI, F., LIENDL, M., LOCKMAN, W., LONGO, F., MAGNI, S., MAIRE, M., MEDERNACH, E., MINAMIMOTO, K., MORA DE FREITAS, P., MORITA, Y., MURAKAMI, K., NAGAMATU, M., NARTALLO, R., NIEMINEN, P., NISHIMURA, T., OHTSUBO, K., OKAMURA, M., O'NEALE, S., OOHATA, Y., PAECH, K., PERL, J., PFEIFFER, A., PIA, M. G., RANJARD, F., RYBIN, A., SADILOV, S., DI SALVO, E., SANTIN, G., SASAKI, T., SAVVAS, N., SAWADA, Y., SCHERER, S., SEI, S., SIROTENKO, V., SMITH, D., STARKOV, N., STOECKER, H., SULKIMO, J., TAKAHATA, M., TANAKA, S., TCHERNIAEV, E., SAFAI TEHRANI, E., TROPEANO, M., TRUSCOTT, P., UNO, H., URBAN, L., URBAN, P., VERDERI, M., WALKDEN, A., WANDER, W., WEBER, H., WELLISCH, J. P., WENAUS, T., WILLIAMS, D. C., WRIGHT, D., YAMADA, T., YOSHIDA, H. and ZSCHIESCHE, D. GEANT4 - A simulation toolkit. *Nuclear Instruments and Methods in Physics Research, Section A: Accelerators, Spectrometers, Detectors and Associated Equipment*. 2003. Vol. 506, no. 3, p. 250–303. DOI 10.1016/S0168-9002(03)01368-8.

43. POON, E, LE, Y, WILLIAMSON, J F and VERHAEGEN, F. BrachyGUI: an adjunct to an accelerated Monte Carlo photon transport code for patient-specific brachytherapy dose calculations and analysis. *Journal of Physics: Conference Series* [online]. 1 February 2008. Vol. 102, no. 1, p. 12018. [Accessed 1 May 2017]. DOI 10.1088/1742-6596/102/1/012018. Available from: http://stacks.iop.org/1742-6596/102/i=1/a=012018?key=crossref.6c2937a2f3e652b0f614f81a1d240871

44. MIKELL, Justin K. and MOURTADA, Firas. Dosimetric impact of an I192r brachytherapy source cable length modeled using a grid-based Boltzmann transport equation solver. *Medical Physics* [online]. 17 August 2010. Vol. 37, no. 9, p. 4733–4743. [Accessed 1 May 2017]. DOI 10.1118/1.3478278. Available from: http://www.ncbi.nlm.nih.gov/pubmed/20964191

45. VARIAN ONCOLOGY. Acuros ® BV advanced dose calculation for brachytherapy 1 |. [online]. [Accessed 1 May 2017]. Available from: https://www.varian.com/oncology/products/software/treatment-planning/acuros-bv-advanced-dose-calculation

46. BEAULIEU, Luc, CARLSSON TEDGREN, Åsa, CARRIER, Jean-François, DAVIS, Stephen D, MOURTADA, Firas, RIVARD, Mark J, THOMSON, Rowan M, VERHAEGEN, Frank, WAREING, Todd A and WILLIAMSON, Jeffrey F. Report of the Task Group 186 on model-based dose calculation methods in brachytherapy beyond the TG-43 formalism: Current status and recommendations for clinical implementation. [online]. [Accessed 1 May 2017]. Available from: https://www.aapm.org/pubs/reports/RPT_186.pdf

47. AHNESJÖ, Anders, VAN VEELEN, Bob and TEDGREN, Åsa Carlsson. Collapsed cone dose calculations for heterogeneous tissues in brachytherapy using primary and scatter separation source data. *Computer Methods and Programs in Biomedicine* [online]. February 2017. Vol. 139, no. C, p. 17–29. [Accessed 1 May 2017]. DOI 10.1016/j.cmpb.2016.10.022. Available from: http://linkinghub.elsevier.com/retrieve/pii/S0169260716303121

48. HADAD, K, ZOHREVAND, M, FAGHIHI, R and A, Sedighi Pashaki. Accuracy evaluation of Oncentra TPS in HDR Brachytherapy of Nasopharynx cancer suing EGSnrc Monte Carlo Code. *Biomedical Physics and Engineering*. 2015. Vol. 5, no. 1, p. 25–30.

49. PAPAGIANNIS, P, PANTELIS, E and KARAISKOS, P. Current state of the art brachytherapy treatment planning dosimetry algorithms. *The British journal of radiology* [online]. September 2014. Vol. 87,

no. 1041, p. 20140163. [Accessed 1 May 2017]. DOI 10.1259/bjr.20140163. Available from: http://www.ncbi.nlm.nih.gov/pubmed/25027247

50. SALGAONKAR, VA, WOOTTON, J and PRAKASH, P. Thermal dosimetry analysis combined with patient-specific thermal modeling of clinical interstitial ultrasound hyperthermia integrated within HDR brachytherapy for. *AIP Conference* [online]. 2017. [Accessed 27 April 2017]. Available from: http://aip.scitation.org/doi/abs/10.1063/1.4977615
51. PAPPAS, ET and MARIS, TG. System and method for patient-specific radiotherapy treatment verification and quality assurance system. *US Patent App. 15/067,333* [online]. 2016. [Accessed 27 April 2017]. Available from: https://www.google.com/patents/US20160256711
52. BRAAD, PE, XIE, T and ZAIDI, H. Implementation, validation, and optimization of 124I-PET Monte Carlo patient specific dosimetry in radioiodine therapy. *Journal of Nuclear* [online]. 2016. [Accessed 27 April 2017]. Available from: http://jnm.snmjournals.org/content/57/supplement_2/496.short
53. SHANTA, A. Need of independent dose verification in brachytherapy. *Journal of medical physics* [online]. July 2008. Vol. 33, no. 3, p. 83–4. [Accessed 27 April 2017]. DOI 10.4103/0971-6203.42743. Available from: http://www.ncbi.nlm.nih.gov/pubmed/19893697
54. NRC: Regulations Title 10, Code of Federal Regulations. [online]. [Accessed 27 April 2017]. Available from: https://www.nrc.gov/reading-rm/doc-collections/cfr/
55. Directive 2013/59/Euratom - protection against ionising radiation - Safety and health at work - EU-OSHA. [online]. [Accessed 27 April 2017]. Available from: https://osha.europa.eu/es/legislation/directives/directive-2013-59-euratom-protection-against-ionising-radiation
56. SMYTH, V, BOBIN, C and LASSMANN, M. Metrology for clinical implementation of dosimetry in molecular radiotherapy: a new EURAMET project. *and Molecular …* [online]. 2016. [Accessed 27 April 2017]. Available from: http://christie.openrepository.com/christie/handle/10541/620198
57. FLUX, GD, O'SULLIVAN, J and GAZE, MN. Commentary Opportunities for research in molecular radiotherapy. *The British Journal of* [online]. 2017. [Accessed 27 April 2017]. Available from: http://www.birpublications.org/doi/abs/10.1259/bjr.20160921
58. BARDIÈS, M. Patient-specific dosimetry in molecular radiotherapy: Why and how? *Physica Medica* [online]. 2016. [Accessed 27 April 2017]. Available from: http://www.sciencedirect.com/science/article/pii/S1120179716304744
59. SAFIAN, N A M, ABDULLAH, N H, ABDULLAH, R and CHIANG, C S. Verification of Oncentra brachytherapy planning using independent calculation. *Journal of Physics: Conference Series* [online]. March 2016. Vol. 694, no. 1, p. 12003. [Accessed 27 April 2017]. DOI 10.1088/1742-6596/694/1/012003. Available from: http://stacks.iop.org/1742-6596/694/i=1/a=012003?key=crossref.8539ce249f899057ade03c1aa4b72efc
60. GADHI, Muhammad, FATMI, Shahab, SHAKIL, Muhammad and BUZDAR, Saeed Ahmad. A method for verification of treatment times for high-dose-rate intraluminal brachytherapy treatment. *International Journal of Cancer Therapy and Oncology* [online]. 30 June 2016. Vol. 4, no. 2, p. 423. [Accessed 3 May 2017]. DOI 10.14319/ijcto.42.3. Available from: http://ijcto.org/index.php/IJCTO/article/view/jcto.42.3
61. CARMONA, Vicente, PEREZ-CALATAYUD, Jose, LLISO, Françoise, RICHART, Jose, BALLESTER, Facundo, PUJADES-CLAUMARCHIRANT, Ma Carmen and VENSELAAR, Jack L.M. Physics

Contributions A program for the independent verification of brachytherapy planning system calculations. *Journal of Contemporary Brachytherapy* [online]. 2010. Vol. 3, no. 3, p. 129–133. [Accessed 3 May 2017]. DOI 10.5114/jcb.2010.16924. Available from: http://www.termedia.pl/doi/10.5114/jcb.2010.16924

62. KUMAR, Rajesh, SHARMA, S D, VIJAYKUMAR, C, DESHPANDE, Sudesh, SHARMA, P K, VANDANA, S, PHILOMENA, A and CHILKULWAR, Ravi H. A dose verification method for high-dose-rate brachytherapy treatment plans. *Journal of cancer research and therapeutics* [online]. Vol. 4, no. 4, p. 173–7. [Accessed 3 May 2017]. Available from: http://www.ncbi.nlm.nih.gov/pubmed/19052390
63. SAFIAN, N A M, ABDULLAH, N H, ABDULLAH, R and CHIANG, C S. Verification of Oncentra brachytherapy planning using independent calculation. *Journal of Physics: Conference Series* [online]. March 2016. Vol. 694, no. 1, p. 12003. [Accessed 3 May 2017]. DOI 10.1088/1742-6596/694/1/012003. Available from: http://stacks.iop.org/1742-6596/694/i=1/a=012003?key=crossref.8539ce249f899057ade03c1aa4b72efc
64. NIKOOFAR, Alireza, HOSEINPOUR, Zohreh, RABI MAHDAVI, Seied, HASANZADEH, Hadi and REZAEI TAVIRANI, Mostafa. High-Dose-Rate (192)Ir Brachytherapy Dose Verification: A Phantom Study. *Iranian journal of cancer prevention* [online]. May 2015. Vol. 8, no. 3, p. e2330. [Accessed 3 May 2017]. DOI 10.17795/ijcp2330. Available from: http://www.ncbi.nlm.nih.gov/pubmed/26413250
65. DAHOUD, MSA and MUSTAFA, IS. Radiation Dosimetry By Tlds Inside Human Body Phantom While Using 192 Ir HDR In Breast Brachytherapy. *International Journal of Scientific & Technology* [online]. 2014. [Accessed 3 May 2017]. Available from: http://www.ijstr.org/final-print/dec2014/Radiation-Dosimetry-By-Tlds-Inside-Human-Body-Phantom-While-Using-192ir-Hdr-In-Breast-Brachytherapy.pdf
66. CHOFOR, N, LOHMANN, N, LUETJENS, S and HARDER, D. SU- E- T- 54: Dosimetric Verification of Monte Carlo Dose Calculations for a GammaMed HDR 192Ir Brachytherapy Source Using Various Detector Types, and Non- . *Medical* [online]. 2013. [Accessed 3 May 2017]. Available from: http://onlinelibrary.wiley.com/doi/10.1118/1.4814489/full
67. MANNING, S and NYATHI, T. An investigation into the accuracy of AcurosTM BV in heterogeneous phantoms for a 192Ir HDR source using LiF TLDs. *Australasian physical & engineering sciences in* [online]. 2014. [Accessed 3 May 2017]. Available from: http://link.springer.com/article/10.1007/s13246-014-0279-4
68. KOZŁOWSKA, B, PALUCH-FERSZT, M and DYBEK, M. Verification of treatment plans for skin cancer in brachytherapy with the use of TLD technique. *Physica Medica* [online]. 2016. [Accessed 3 May 2017]. Available from: http://www.sciencedirect.com/science/article/pii/S1120179716307360
69. ADLIENE, Diana, JAK??TAS, Karolis and URBONAVI??IUS, Benas Gabrielis. In Vivo TLD dose measurements in catheter-based high-dose-rate brachytherapy. *Radiation Protection Dosimetry* [online]. July 2015. Vol. 165, no. 1–4, p. 477–481. [Accessed 3 May 2017]. DOI 10.1093/rpd/ncv054. Available from: http://www.ncbi.nlm.nih.gov/pubmed/25809111
70. GAMBARINI, G., BORRONI, M., GRISOTTO, S., MAUCIONE, A., CERROTTA, A., FALLAI, C. and CARRARA, M. Solid state TL detectors for in vivo dosimetry in brachytherapy. *Applied Radiation and Isotopes* [online]. December 2012. Vol. 71, no. SUPPL., p. 48–51. [Accessed 3 May 2017]. DOI 10.1016/j.apradiso.2012.06.018. Available from: http://www.ncbi.nlm.nih.gov/pubmed/22920417
71. NAKANO, T, SUCHOWERSKA, N, MCKENZIE, D R and BILEK, M M. Real-time verification of HDR brachytherapy source location: implementation of detector redundancy. *Physics in Medicine and Biology*

[online]. 21 January 2005. Vol. 50, no. 2, p. 319–327. [Accessed 3 May 2017]. DOI 10.1088/0031-9155/50/2/010. Available from: http://stacks.iop.org/0031-9155/50/i=2/a=010?key=crossref.546b6ac02a7e851d708c5b4540378120

72. UNIYAL, S. C., SHARMA, S. D. and NAITHANI, U. C. A dosimetry method in the transverse plane of HDR Ir-192 brachytherapy source using gafchromic EBT2 film. *Physica Medica* [online]. April 2012. Vol. 28, no. 2, p. 129–133. [Accessed 3 May 2017]. DOI 10.1016/j.ejmp.2011.03.005. Available from: http://www.ncbi.nlm.nih.gov/pubmed/21507693
73. MANIKANDAN, A, BIPLAB, Sarkar, DAVID, Perianayagam A, HOLLA, R, VIVEK, T R and SUJATHA, N. Relative dosimetrical verification in high dose rate brachytherapy using two-dimensional detector array IMatriXX. *Journal of medical physics* [online]. July 2011. Vol. 36, no. 3, p. 171–5. [Accessed 3 May 2017]. DOI 10.4103/0971-6203.83491. Available from: http://www.ncbi.nlm.nih.gov/pubmed/21897562
74. JAREMA, T., CUTAJAR, D., WEAVER, M., PETASECCA, M., LERCH, M., KEJDA, A. and ROSENFELD, A. Dose verification of eye plaque brachytherapy using spectroscopic dosimetry. *Australasian Physical & Engineering Sciences in Medicine* [online]. 19 September 2016. Vol. 39, no. 3, p. 627–632. [Accessed 3 May 2017]. DOI 10.1007/s13246-016-0453-y. Available from: http://link.springer.com/10.1007/s13246-016-0453-y
75. WEAVER, Michael R. Dose Verification for Ophthalmic Brachytherapy Plaque Quality Assurance. [online]. 2015. [Accessed 3 May 2017]. Available from: http://ro.uow.edu.au/theses/4389/
76. VANDECASTEELE, Jan and DE DEENE, Yves. Evaluation of radiochromic gel dosimetry and polymer gel dosimetry in a clinical dose verification. *Physics in Medicine and Biology* [online]. 21 September 2013. Vol. 58, no. 18, p. 6241–6262. [Accessed 3 May 2017]. DOI 10.1088/0031-9155/58/18/6241. Available from: http://www.ncbi.nlm.nih.gov/pubmed/23965800
77. ADLIENE, Diana, JAKSTAS, K., VAICIUNAITE, N., LAURIKAITIENE, J. and CERAPAITE-TRUSINSKIENE, R. Application of dose gels in HDR brachytherapy. In : *IFMBE Proceedings* [online]. Springer, Cham, 2015. p. 724–727. [Accessed 3 May 2017]. ISBN 9783319193878. Available from: http://link.springer.com/10.1007/978-3-319-19387-8_178
78. FARAJOLLAHI, A R, BONNETT, D E, RATCLIFFE, A J, AUKETT, R J and MILLS, J A. An investigation into the use of polymer gel dosimetry in low dose rate brachytherapy. *The British journal of radiology* [online]. November 1999. Vol. 72, no. 863, p. 1085–92. [Accessed 3 May 2017]. DOI 10.1259/bjr.72.863.10700826. Available from: http://www.ncbi.nlm.nih.gov/pubmed/10700826
79. BALDOCK, C. Review of gel dosimetry: a personal reflection. *Journal of Physics: Conference Series* [online]. 2017. [Accessed 3 May 2017]. Available from: http://iopscience.iop.org/article/10.1088/1742-6596/777/1/012029/meta
80. SENKESEN, Oznur, TEZCANLI, Evrim, BUYUKSARAC, Bora and OZBAY, Ismail. Comparison of 3D dose distributions for HDR 192Ir brachytherapy sources with normoxic polymer gel dosimetry and treatment planning system. *Medical dosimetry : official journal of the American Association of Medical Dosimetrists* [online]. 2014. Vol. 39, no. 3, p. 266–71. [Accessed 3 May 2017]. DOI 10.1016/j.meddos.2014.04.003. Available from: http://www.ncbi.nlm.nih.gov/pubmed/24933316
81. WATANABE, Yoichi, WARMINGTON, Leighton and GOPISHANKAR, N. Three-dimensional radiation dosimetry using polymer gel and solid radiochromic polymer: From basics to clinical applications. *World journal of radiology* [online]. 28 March 2017. Vol. 9, no. 3, p. 112–125. [Accessed 3 May 2017]. DOI 10.4329/wjr.v9.i3.112. Available from: http://www.ncbi.nlm.nih.gov/pubmed/28396725

82. PEPPA, V., PAPPAS, E., PANTELIS, E. and PAPAGIANNIS, P. A QA procedure for brachytherapy TPS employing model based dose calculations, based on Monte Carlo simulation and end user oriented tools. *Physica Medica* [online]. 2014. Vol. 30. [Accessed 20 April 2017]. DOI 10.1016/j.ejmp.2014.07.206. Available from: http://www.sciencedirect.com.ezproxy.ktu.edu/science/article/pii/S1120179714003706

83. PANAIT, Roxana, BUTUC, Irina, CONSTANTIN, Cristin, GRIVOLE, Magda and MIHAILESCU, Dan. *Monte Carlo codes for use in medical radiation physics* [online]. [Accessed 3 May 2017]. Available from: http://www.academia.edu/5146039/Monte_Carlo_codes_for_medical_radiation_physics

84. X-5 MONTE CARLO TEAM. MCNP - A General Monte Carlo N-Particle Transport Code, Version 5. *Los Alamos Nuclear Laboratory*. 2005. Vol. I, p. 2-71-2–80. DOI LA-UR-03-1987.

85. ZHANG, Hualin and DAS, Indra J. Dosimetric perturbations at high-Z interfaces with high dose rate 192Ir source. *Physica Medica* [online]. 2014. Vol. 30, no. 7, p. 782–790. [Accessed 20 April 2017]. DOI 10.1016/j.ejmp.2014.06.005. Available from: http://www.sciencedirect.com.ezproxy.ktu.edu/science/article/pii/S1120179714001094

86. WU, C H, LIAO, Y J, LIU, Y W Hsueh, HUNG, S K, LEE, M S and HSU, S M. Dose distributions of an ^{192}Ir brachytherapy source in different media. *BioMed research international* [online]. 2014. Vol. 2014, p. 946213. [Accessed 20 April 2017]. DOI 10.1155/2014/946213. Available from: http://www.ncbi.nlm.nih.gov/pubmed/24804263

87. MOUTSATSOS, A., PANTELIS, E., PAPPAS, E. and PAPAGIANNIS, P. Experimental dosimetry for model-based 192Ir HDR brachytherapy treatment planning. *Physica Medica* [online]. 2014. Vol. 30. [Accessed 20 April 2017]. DOI 10.1016/j.ejmp.2014.07.112. Available from: http://www.sciencedirect.com.ezproxy.ktu.edu/science/article/pii/S1120179714002762

88. EGS4, Electron Photon Shower Simulation by Monte-Carlo. [online]. [Accessed 3 May 2017]. Available from: http://www.oecd-nea.org/tools/abstract/detail/ccc-0331/

89. SALVAT, F, FERNÁNDEZ-VAREA, JM and SEMPAU, J. PENELOPE-2011: a code system for Monte Carlo simulation of electron and photon transport OECD NEA Data Bank. *NSC DOC (2011)/5 (Issy-les-Moulineaux:* [online]. 2011. [Accessed 4 May 2017]. Available from: https://scholar.google.lt/scholar?q=PENELOPE-2011%3A+A+Code+System+for+Monte+Carlo+Simulation+of+Electron+and+Photon+Transport&hl=lt&as_sdt=0%2C5&as_ylo=2010&as_yhi=

90. JIA, Xun, GU, Xuejun, SEMPAU, Josep, CHOI, Dongju, MAJUMDAR, Amitava and JIANG, Steve B. Development of a GPU-based Monte Carlo dose calculation code for coupled electron–photon transport. *Physics in Medicine and Biology* [online]. 7 June 2010. Vol. 55, no. 11, p. 3077–3086. [Accessed 4 May 2017]. DOI 10.1088/0031-9155/55/11/006. Available from: http://stacks.iop.org/0031-9155/55/i=11/a=006?key=crossref.59391a5ade5c978deda25ee635a146dc

91. SEMPAU, Josep, WILDERMAN, Scott J and BIELAJEW, Alex F. DPM, a fast, accurate Monte Carlo code optimized for photon and electron radiotherapy treatment planning dose calculations. *Physics in Medicine and Biology* [online]. 1 August 2000. Vol. 45, no. 8, p. 2263–2291. [Accessed 4 May 2017]. DOI 10.1088/0031-9155/45/8/315. Available from: http://stacks.iop.org/0031-9155/45/i=8/a=315?key=crossref.7719915e3555245239f06f275522d73f

92. HISSOINY, Sami, OZELL, Benoît, BOUCHARD, Hugo and DESPRÉS, Philippe. GPUMCD : A new GPU-oriented Monte Carlo dose calculation platform. *Medical Physics* [online]. 13 January 2011. Vol. 38, no. 2, p. 754–764. [Accessed 4 May 2017]. DOI 10.1118/1.3539725. Available from:

http://doi.wiley.com/10.1118/1.3539725

93. SNYDER, WS. Report of the Task Group on Reference Man Report of the Task Group on Reference Man. *Pergamon Press: New York* [online]. [Accessed 19 April 2017]. Available from: https://scholar.google.lt/scholar?q=+Report+of+the+Task+Group+on+Reference+Man%3A+ICRP+Publication+23.&btnG=&hl=en&as_sdt=0%2C5

94. SNYDER, W S, FORD, M R and WARNER, G G. MIRD Pamphlet No. 5: Estimates of absorbed fractions for monoenergetic photon sources uniformly distributed in various organs of a heterogeneous phantom. *Journal of nuclear medicine : official publication, Society of Nuclear Medicine* [online]. 1969. P. Suppl 3:7-52. [Accessed 19 April 2017]. Available from: http://www.osti.gov/scitech/biblio/4750501

95. ZAIDI, H and XU, XG. Computational anthropomorphic models of the human anatomy: the path to realistic Monte Carlo modeling in radiological sciences. *Annu. Rev. Biomed. Eng.* [online]. 2007. [Accessed 19 April 2017]. Available from: http://annualreviews.org/doi/abs/10.1146/annurev.bioeng.9.060906.151934

96. ZUBAL, I.G., HARRELL, C.R., SMITH, E.O., SMITH, a.L. and KRISCHLUNAS, P. Two dedicated software, voxel-based, anthropomorphic (torso and head) phantoms. *Proceeding of the International Conference at the National Radiological Protection Board* [online]. 1995. P. 105–111. [Accessed 19 April 2017]. Available from: http://ipagwww.med.yale.edu/zubal/library/Zubal.pdf

97. ZUBAL, George. Sample Images - Phantom with Legs and Arms Attached. [online]. [Accessed 19 April 2017]. Available from: http://noodle.med.yale.edu/zubal/samplesarmslegs.htm

98. NA, Yong Hum, ZHANG, Binquan, ZHANG, Juying, CARACAPPA, Peter F and XU, X George. Deformable adult human phantoms for radiation protection dosimetry: anthropometric data representing size distributions of adult worker populations and software algorithms. *Physics in medicine and biology* [online]. 2010. Vol. 55, no. 13, p. 3789–811. [Accessed 19 April 2017]. DOI 10.1088/0031-9155/55/13/015. Available from: http://www.ncbi.nlm.nih.gov/pubmed/20551505

99. XU, X George. An exponential growth of computational phantom research in radiation protection, imaging, and radiotherapy: a review of the fifty-year history. *Physics in medicine and biology* [online]. 2014. Vol. 59, no. 18, p. R233–R302. DOI 10.1088/0031-9155/59/18/R233. Available from: http://www.ncbi.nlm.nih.gov/pubmed/25144730

100. ABELLA, V., MIRÓ, R., JUSTE, B. and VERDÚ, G. 3D dose distribution calculation in a voxelized human phantom by means of Monte Carlo method. *Applied Radiation and Isotopes* [online]. 2010. Vol. 68, no. 4, p. 709–713. [Accessed 20 April 2017]. DOI 10.1016/j.apradiso.2009.10.016. Available from: http://www.sciencedirect.com.ezproxy.ktu.edu/science/article/pii/S0969804309006332

101. TELES, P., BARROS, S., CARDOSO, S., FACURE, A., DA ROSA, L. A. R., SANTOS, M., PEREIRA, P., VAZ, P. and ZANKL, M. A dosimetric study of prostate brachytherapy using Monte Carlo simulations with a voxel phantom, measurements and a comparison with a treatment planning procedure. *Radiation Protection Dosimetry* [online]. July 2015. Vol. 165, no. 1–4, p. 482–487. [Accessed 20 April 2017]. DOI 10.1093/rpd/ncv055. Available from: https://academic.oup.com/rpd/article-lookup/doi/10.1093/rpd/ncv055

102. ANJOMROUZ, Marzieh, BAKHT, Mo K. and SADEGHI, Mahdi. Feasibility study of FLUKA Monte Carlo simulation for a beta-emitting brachytherapy source: dosimetric parameters of 142Pr glass seed. *Journal of Radioanalytical and Nuclear Chemistry* [online]. 4 September 2016. Vol. 309, no. 3, p. 947–953. [Accessed 20 April 2017]. DOI 10.1007/s10967-016-4744-2. Available from:

http://link.springer.com/10.1007/s10967-016-4744-2

103. ROBERT, C, DEDES, G and BATTISTONI, G. Distributions of secondary particles in proton and carbon-ion therapy: a comparison between GATE/Geant4 and FLUKA Monte Carlo codes. *Physics in medicine* [online]. 2013. [Accessed 20 April 2017]. Available from: http://iopscience.iop.org/article/10.1088/0031-9155/58/9/2879/meta

104. BÖHLEN, TT, CERUTTI, F, DOSANJH, M and FERRARI, A. Benchmarking nuclear models of FLUKA and GEANT4 for carbon ion therapy. *Physics in medicine* [online]. 2010. [Accessed 20 April 2017]. Available from: http://iopscience.iop.org/article/10.1088/0031-9155/55/19/014/meta

105. PARODI, K, FERRARI, A and SOMMERER, F. Clinical CT-based calculations of dose and positron emitter distributions in proton therapy using the FLUKA Monte Carlo code. *Physics in medicine and* [online]. 2007. [Accessed 20 April 2017]. Available from: http://iopscience.iop.org/article/10.1088/0031-9155/52/12/004/meta

106. BATTISTONI, G, BROGGI, F and BRUGGER, M. The FLUKA code and its use in hadron therapy. *Societa Italiana di …* [online]. 2008. [Accessed 20 April 2017]. Available from: https://sapienza.pure.elsevier.com/it/publications/the-fluka-code-and-its-use-in-hadron-therapy

107. RATA, R, BARLOW, R and LEE, S. FLUKA Simulations for Radiation Protection at 3 Different Facilities. *(IPAC'16), Busan, Korea, May 8- …* [online]. 2016. [Accessed 20 April 2017]. Available from: http://accelconf.web.cern.ch/AccelConf/ipac2016/papers/tupoy018.pdf

108. INFANTINO, A, CICORIA, G, LUCCONI, G, PANCALDI, D and VICHI, S. Assessment of the neutron dose field around a biomedical cyclotron: FLUKA simulation and experimental measurements. *Physica Medica* [online]. 2016. [Accessed 20 April 2017]. Available from: http://www.sciencedirect.com/science/article/pii/S1120179716310870

109. FEHRENBACHER, G, KOZLOVA, E and RADON, T. FLUKA shielding calculations for the FAIR project. *StrahlenschutzPraxis (* [online]. 2015. [Accessed 20 April 2017]. Available from: https://inis.iaea.org/search/search.aspx?orig_q=RN:46130687

110. GUTHOFF, M, BOER, W de and MÜLLER, S. Simulation of beam induced lattice defects of diamond detectors using FLUKA. *and Methods in Physics Research Section …* [online]. 2014. [Accessed 20 April 2017]. Available from: http://www.sciencedirect.com/science/article/pii/S0168900213012291

111. SEN, M, SATHIAN, V, SHOBHA, G and YASHODA, S. Study of various moderator materials to design a collimator for the fast neutron beam using Fluka simulation. *Proceedings of the* [online]. 2016. [Accessed 20 April 2017]. Available from: https://inis.iaea.org/search/search.aspx?orig_q=RN:47088524

112. KUROSU, K, DAS, IJ and MOSKVIN, VP. Optimization of GATE and PHITS Monte Carlo code parameters for spot scanning proton beam based on simulation with FLUKA general-purpose code. *in Physics Research Section B: Beam …* [online]. 2016. [Accessed 20 April 2017]. Available from: http://www.sciencedirect.com/science/article/pii/S0168583X15012008

113. INFANTINO, A, OEHLKE, E, MOSTACCI, D and SCHAFFER, P. Assessment of the production of medical isotopes using the Monte Carlo code FLUKA: simulations against experimental measurements. *Nuclear Instruments and* [online]. 2016. [Accessed 20 April 2017]. Available from: http://www.sciencedirect.com/science/article/pii/S0168583X15010976

114. FERRARI, A. FLUKA: from LHC to medical applications. . 2014.

115. HANEEFA, K Abdul, CYRIAC, TS and MUSTHAFA, MM. FLUKA Monte Carlo for Basic Dosimetric

Studies of Dual Energy Medical Linear Accelerator. *Journal of* [online]. 2014. [Accessed 20 April 2017]. Available from: https://www.hindawi.com/archive/2014/343979/abs/

116. BÖHLEN, TT, CERUTTI, F, CHIN, MPW, FASSÒ, A and FERRARI, A. The FLUKA code: developments and challenges for high energy and medical applications. *Nuclear Data* [online]. 2014. [Accessed 20 April 2017]. Available from: http://www.sciencedirect.com/science/article/pii/S0090375214005018
117. BALLARINI, F, BATTISTONI, G, CAMPANELLA, M, CARBONI, M, CERUTTI, F, EMPL, A, FASSÒ, A, FERRARI, A, GADIOLI, E, GARZELLI, M V, LANTZ, M, LIOTTA, M, MAIRANI, A, MOSTACCI, A, MURARO, S, OTTOLENGHI, A, PELLICCIONI, M, PINSKY, L, RANFT, J, ROESLER, S, SALA, P R, SCANNICCHIO, D, TROVATI, S, VILLARI, R, WILSON, T, ZAPP, N and VLACHOUDIS, V. The FLUKA code: an overview. *Journal of Physics: Conference Series* [online]. 1 May 2006. Vol. 41, no. 1, p. 151–160. [Accessed 25 March 2017]. DOI 10.1088/1742-6596/41/1/014. Available from: http://stacks.iop.org/1742-6596/41/i=1/a=014?key=crossref.0b9bcd803fa351dbf46abb9e7dcd9558
118. HTTP://WWW.FLUKA.ORG/FLUKA.PHP. The official FLUKA site: FLUKA home. [online]. 2015. [Accessed 25 March 2017]. Available from: http://www.fluka.org/fluka.php
119. IWABUCHI, H. Efficient Monte Carlo methods for radiative transfer modeling. *Journal of the atmospheric sciences* [online]. 2015. [Accessed 16 April 2017]. Available from: http://journals.ametsoc.org/doi/abs/10.1175/JAS3755.1
120. KLING, A, BARAO, FJC, NAKAGAWA, M, TAVORA, L and VAZ, P. *Advanced Monte Carlo for Radiation Physics, Particle Transport Simulation and Applications: Proceedings of the Monte Carlo 2000 Conference, Lisbon, 23–* [online]. 2014. [Accessed 16 April 2017]. Available from: https://www.google.com/books?hl=en&lr=&id=cLDCBAAAQBAJ&oi=fnd&pg=PR3&dq=particle+transport+boltzmann&ots=73ctqOI8bu&sig=abk2JZD-lV6v9fPOwXo6XIyYgGs
121. PÉRAUD, JPM and LANDON, CD. Monte Carlo methods for solving the Boltzmann transport equation. *Annual Review of Heat* [online]. 2014. [Accessed 16 April 2017]. Available from: http://www.dl.begellhouse.com/pt/download/article/1d883b612ccfafde/ARHT(7)-7381.pdf
122. RUBINSTEIN, RY and KROESE, DP. Simulation and the Monte Carlo method. . 2016.
123. BERGER, MJ. Monte Carlo calculation of the penetration and diffusion of fast charged particles. *Methods in Computational Physics* [online]. 1963. Vol. 1, p. 135–215. [Accessed 16 April 2017]. Available from: https://scholar.google.lt/scholar?q=Berger%2C+M.+J.+1963.+Monte+Carlo+calculation+of+the+penetration+and+diffusion+of+fast+charged+particles&btnG=&hl=en&as_sdt=0%2C5&as_ylo=1960&as_yhi=1965
124. KAWRAKOW, I. Accurate condensed history Monte Carlo simulation of electron transport. II. Application to ion chamber response simulations. *Medical Physics* [online]. March 2000. Vol. 27, no. 3, p. 499–513. [Accessed 16 April 2017]. DOI 10.1118/1.598918. Available from: http://www.ncbi.nlm.nih.gov/pubmed/10757602
125. RIBBERFORS, R and CARLSSON, GA. Compton component of the mass-energy absorption coefficient: corrections due to the energy broadening of compton-scattered photons. *Radiation research* [online]. 1985. [Accessed 19 April 2017]. Available from: http://www.rrjournal.org/doi/abs/10.2307/3576302
126. HUBBELL, J H. Review of photon interaction cross section data in the medical and biological context. *Physics in medicine and biology* [online]. 1999. Vol. 44, no. 1, p. R1–R22. [Accessed 19 April 2017]. DOI 10.1088/0031-9155/44/1/001. Available from: http://iopscience.iop.org/article/10.1088/0031-9155/44/1/001/meta

127. VIANA, Rodrigo Sartorelo Salemi, FLORENTINO, Helenice de Oliveira, LIMA, Ernesto Augusto Bueno da Fonseca, FONSECA, Paulo Roberto da and HOMEM, Thiago Pedro Donadon. Heterogeneity correction in the construction of optimized planning in radiotherapy using linear programming. *Pesquisa Operacional* [online]. December 2011. Vol. 31, no. 3, p. 565–578. [Accessed 19 April 2017]. DOI 10.1590/S0101-74382011000300009. Available from: http://www.scielo.br/scielo.php?script=sci_arttext&pid=S0101-74382011000300009&lng=en&nrm=iso&tlng=en

128. GOLDSTONE, K. E. Tissue Substitutes in Radiation Dosimetry and Measurement, in: ICRU Report 44. International Commission on Radiation Units and Measurements, USA (1989). *Clinical Radiology* [online]. 1990. Vol. 41, no. 3, p. 220. [Accessed 19 April 2017]. DOI 10.1016/S0009-9260(05)80988-2. Available from: http://www.researchgate.net/publication/256686573_Tissue_Substitutes_in_Radiation_Dosimetry_and_Measurement_in_ICRU_Report_44._International_Commission_on_Radiation_Units_and_Measurements_USA_(1989)

129. BEAULIEU, L, TEDGREN, Å Carlsson and CARRIER, JF. Report of the Task Group 186 on model- based dose calculation methods in brachytherapy beyond the TG- 43 formalism: Current status and recommendations for. *Medical* [online]. 2012. [Accessed 19 April 2017]. Available from: http://onlinelibrary.wiley.com/doi/10.1118/1.4747264/full

130. PEREZ-CALATAYUD, Jose, BALLESTER, Facundo, DAS, Rupak K., DEWERD, Larry a., IBBOTT, Geoffrey S., MEIGOONI, Ali S., OUHIB, Zoubir, RIVARD, Mark J., SLOBODA, Ron S. and WILLIAMSON, Jeffrey F. Dose calculation for photon-emitting brachytherapy sources with average energy higher than 50 keV: Report of the AAPM and ESTRO. *Medical Physics* [online]. 2012. Vol. 39, no. 5, p. 2904–2929. [Accessed 19 March 2017]. DOI 10.1118/1.3703892. Available from: http://scitation.aip.org/content/aapm/journal/medphys/39/5/10.1118/1.3703892

131. HERRERA-MARTÍNEZ, Adonai and KADI, Yacine. Accelerator-Driven System Design FLUKA Exercise. *Organization* [online]. 2005. P. 1–20. [Accessed 25 March 2017]. Available from: http://indico.ictp.it/event/a04210/session/14/contribution/8/material/0/1.pdf

132. MITAROFF, A. and SILARI, M. The CERN-EU High-energy Reference Field (CERF) Facility for Dosimetry at Commercial Flight Altitudes and in Space. *Radiation Protection Dosimetry* [online]. 1 September 2002. Vol. 102, no. 1, p. 7–22. [Accessed 25 March 2017]. DOI 10.1093/oxfordjournals.rpd.a006075. Available from: https://academic.oup.com/rpd/article-lookup/doi/10.1093/oxfordjournals.rpd.a006075

133. The official FLUKA site: FLUKA Online Manual. [online]. [Accessed 25 March 2017]. Available from: http://www.fluka.org/fluka.php?id=man_onl&sub=3

134. FERRARI, A, SALA, P R, GUARALDI, R and PADOANI, F. An improved multiple scattering model for charged particle transport. *Nucl. Inst. Meth.* [online]. 1992. Vol. B71, p. 412–416. [Accessed 20 April 2017]. Available from: http://www.sciencedirect.com/science/article/pii/0168583X9295359Y

135. BATTISTONI, G., CERUTTI, F., FASSÒ, A., FERRARI, A., MURARO, S., RANFT, J., ROESLER, S. and SALA, P. R. The FLUKA code: Description and benchmarking. *AIP Conference Proceedings* [online]. 2007. Vol. 896, p. 31–49. [Accessed 20 April 2017]. DOI 10.1063/1.2720455. Available from: http://aip.scitation.org/doi/abs/10.1063/1.2720455

136. FANO, U., MCVOY, K. W. and ALBERS, James R. Sauter theory of the photoelectric effect. *Physical Review* [online]. 1 December 1959. Vol. 116, no. 5, p. 1147–1156. [Accessed 20 April 2017].

DOI 10.1103/PhysRev.116.1147. Available from: https://link.aps.org/doi/10.1103/PhysRev.116.1147

137. BATTISTONI, Giuseppe, BAUER, Julia, BOEHLEN, Till T, CERUTTI, Francesco, CHIN, Mary P W, DOS SANTOS AUGUSTO, Ricardo, FERRARI, Alfredo, ORTEGA, Pablo G, KOZŁOWSKA, Wioletta, MAGRO, Giuseppe, MAIRANI, Andrea, PARODI, Katia, SALA, Paola R, SCHOOFS, Philippe, TESSONNIER, Thomas and VLACHOUDIS, Vasilis. The FLUKA Code: An Accurate Simulation Tool for Particle Therapy. *Frontiers in oncology* [online]. 11 May 2016. Vol. 6, p. 116. [Accessed 20 April 2017]. DOI 10.3389/fonc.2016.00116. Available from: http://journal.frontiersin.org/article/10.3389/fonc.2016.00116/abstract

138. ANDERSEN, V., BALLARINI, F., BATTISTONI, G., CAMPANELLA, M., CARBONI, M., CERUTTI, F., EMPL, A., FASSÒ, A., FERRARI, A., GADIOLI, E., GARZELLI, M. V., LEE, K., OTTOLENGHI, A., PELLICCIONI, M., PINSKY, L. S., RANFT, J., ROESLER, S., SALA, P. R. and WILSON, T. L. The FLUKA code for space applications: Recent developments. *Advances in Space Research* [online]. 2004. Vol. 34, no. 6, p. 1302–1310. [Accessed 20 April 2017]. DOI 10.1016/j.asr.2003.03.045. Available from: http://www.sciencedirect.com/science/article/pii/S0273117704002054

139. OAC "HPC Saulėtekis" | VU superkompiuteriai. [online]. [Accessed 20 April 2017]. Available from: http://www.supercomputing.vu.lt/en/hpc-sauletekis/

140. SHULTIS, J K and FAW, R E. AN MCNP PRIMER. [online]. [Accessed 26 March 2017]. Available from: http://www.mne.k-state.edu/~jks/MCNPprmr.pdf

141. MCNP MANUAL. *Version 2.5. 0, April, 2005*. [no date].

142. JUDITH F. BRIESMEISTER. *MCNP–A General Monte Carlo N–Particle Transport Code* [online]. 2000. [Accessed 26 March 2017]. Available from: http://permalink.lanl.gov/object/tr?what=info:lanl-repo/lareport/LA-13709-M

143. VLACHOUDIS, V. FLAIR: A Powerful But User Friendly Graphical Interface For FLUKA. *Proc. Int. Conf. on Mathematics, Computational* [online]. 2009. P. 1–11. [Accessed 23 June 2016]. Available from: http://www.fluka.org/FLUKA/flair/Flair_MC2009.pdf

144. THEIS, C., BUCHEGGER, K.H., BRUGGER, M., FORKEL-WIRTH, D., ROESLER, S. and VINCKE, H. Interactive three-dimensional visualization and creation of geometries for Monte Carlo calculations. *Nuclear Instruments and Methods in Physics Research Section A: Accelerators, Spectrometers, Detectors and Associated Equipment* [online]. June 2006. Vol. 562, no. 2, p. 827–829. [Accessed 23 June 2016]. DOI 10.1016/j.nima.2006.02.125. Available from: http://linkinghub.elsevier.com/retrieve/pii/S0168900206003056

145. BORG, J and ROGERS, DWO. Monte Carlo calculations of photon spectra in air from 192Ir sources. *National Research Council Report PIRS-629r, Ontario,*. 1999.

146. RODRIGUES, Sane Simone Oliveira Fonseca, BEGALLI, Marcia, FILHO, Pedro Pacheco de Queiroz and DE SOUZA SANTOS, Denison. Monte Carlo simulation of an Ir-192 brachytherapy source spectra, geometry and anysotropy factors using GEANT4 code. In : *2008 IEEE Nuclear Science Symposium Conference Record* [online]. IEEE, October 2008. p. 860–863. [Accessed 8 May 2017]. ISBN 978-1-4244-2714-7. Available from: http://ieeexplore.ieee.org/document/4774530/

147. WOODARD, H Q and WHITE, D R. The composition of body tissues. *The British journal of radiology* [online]. 1991. Vol. 64, p. 149–159. [Accessed 20 April 2017]. DOI 10.1259/0007-1285-59-708-1209. Available from: http://www.birpublications.org/doi/abs/10.1259/0007-1285-59-708-1209

8. APPENDICES

APPENDIX A

```
TITLE
GLOBAL        1000.0       0.0       0.0       0.0       1.0        0.
DEFAULTS                                                              PRECISIO
BEAM                                                                  ISOTOPE
BEAMPOS          0.0       0.0       0.0
BEAMPOS                  0.065                 0.36                   CYLI-VOL
HI-PROPE         77.      192.
GEOBEGIN                                                              COMBNAME
    0    0                    MC-CAD
* ASphere2
SPH Sphere     0.00 0.00 0.00 150.
* extvoid
SPH extvoid    0.00 0.00 0.00 1000.00
* intvoid
SPH intvoid    0.00 0.00 0.00 500.00
* shell1
RCC shell1     0.00 0.00 -0.18 0.00 0.00 0.45 0.09
* shell2
RCC shell2     0.0 0.0 0.27 0.0 0.0 0.2 0.07
* shell3
SPH shell3     0.00 0.00 -0.18 0.09
* source
RCC source     0.00 0.00 -0.17 0.00 0.00 0.36 0.065
END
* Reg # 1
* BLACKHOL; assigned material: Blackhole; mat # (1)
BLACKHOL     5 +extvoid  -intvoid
* Reg # 2
* void; assigned material: Vacuum; mat # (2)
VOID         5 +intvoid  -Sphere
* Reg # 4
* AIR1; assigned material: Air; mat # (29)
SPHERE       5 +Sphere  -shell1  -shell2  -shell3
* Reg # 5
* STEEL; assigned material: SS316LN; mat # (27)
STEEL        5 +shell1  -source | +shell2 | +shell3  -source
* Reg # 6
* IRIDIUM; assigned material: IRIDIUM; mat # (28)
IRIDIUM      5 +source
END
GEOEND
MATERIAL         77.               22.42                              IRIDIUM
MATERIAL         24.                7.18                              CHROMIUM
MATERIAL         25.                7.21                              MANGANES
MATERIAL         15.                1.82                              PHOSPHO
MATERIAL         16.                2.07                              SULFUR
* Steel316LN
* Stainless steel AISI316LN
MATERIAL                            7.8                                SS316LN
COMPOUND    -0.67145      IRON    -0.185  CHROMIUM   -0.1125    NICKELSS316LN
COMPOUND       -0.02  MANGANES     -0.01   SILICON  -0.00045   PHOSPHOSS316LN
COMPOUND     -0.0003    SULFUR   -0.0003    CARBON                    SS316LN
MATERIAL         78.               21.45                              PLATINUM
* Ir192
*
```

```
MATERIAL                          21.78                                 Ir192
COMPOUND        -0.3   IRIDIUM      -0.7  PLATINUM                       Ir192
* 104 Air dry (near sea level)
*
MATERIAL                        .00120484                               AIR
COMPOUND   -1.248E-4    CARBON -0.755267  NITROGEN -0.231781    OXYGENAIR
COMPOUND   -0.012827     ARGON                                        AIR
ASSIGNMA    BLCKHOLE  BLACKHOL
ASSIGNMA      VACUUM      VOID
ASSIGNMA       WATER    SPHERE
ASSIGNMA     SS316LN     STEEL
ASSIGNMA       Ir192   IRIDIUM
RADDECAY          2.
DCYSCORE         -1.                        regdose     dose2          USRBIN
DCYSCORE         -1.                          energ     energ          USRTRACK
USRBIN           10.      DOSE      -40.      150.      150.      150.regdose
USRBIN         -150.     -150.     -150.      300.      300.      300. &
USRBIN           11.      DOSE      -41.      150.       0.0      150.dose
USRBIN           0.0       0.0     -150.      600.        1.      600. &
USRBIN           11.      DOSE      -42.      150.       0.0      150.dose1
USRBIN           0.0       0.0     -150.      300.        1.      300. &
USRBIN           11.      DOSE      -43.       15.       0.0       15.dose2
USRBIN           0.0       0.0      -15.      300.        1.      300. &
USRTRACK         -1.    ENERGY      -60.    SPHERE                500.energ
USRTRACK        1E-2      1E-5                                          &
RANDOMIZ          1.
START            1E9
STOP
```

APPENDIX B

```
TITLE
GLOBAL        1000.0       0.0       0.0       0.0       1.0        0.
DEFAULTS                                                              PRECISIO
BEAM                                                                  ISOTOPE
BEAMPOS          0.0       0.0       0.0
BEAMPOS                  0.065                 0.36                   CYLI-VOL
HI-PROPE         77.      192.
GEOBEGIN                                                              COMBNAME
    0    0                    MC-CAD
SPH Sphere     0.00 0.00 0.00 30.
SPH extvoid    0.00 0.00 0.00 1000.00
SPH intvoid    0.00 0.00 0.00 500.00
RCC shell1     0.00 0.00 -0.18 0.00 0.00 0.45 0.09
RCC shell2     0.0 0.0 0.27 0.0 0.0 0.2 0.07
SPH shell3     0.00 0.00 -0.18 0.09
RCC source     0.00 0.00 -0.17 0.00 0.00 0.36 0.065
END
BLACKHOL     5 +extvoid  -intvoid
VOID         5 +intvoid  -Sphere
SPHERE       5 +Sphere  -shell1  -shell2  -shell3
STEEL        5 +shell1  -source | +shell2 | +shell3  -source
IRIDIUM      5 +source
END
GEOEND
MATERIAL         77.               22.42                              IRIDIUM
MATERIAL         24.                7.18                              CHROMIUM
MATERIAL         25.                7.21                              MANGANES
MATERIAL         15.                1.82                              PHOSPHO
MATERIAL         16.                2.07                              SULFUR
* Steel316LN
* Stainless steel AISI316LN
MATERIAL                            7.8                                SS316LN
COMPOUND    -0.67145      IRON    -0.185  CHROMIUM   -0.1125    NICKELSS316LN
COMPOUND       -0.02  MANGANES     -0.01   SILICON  -0.00045   PHOSPHOSS316LN
COMPOUND     -0.0003    SULFUR   -0.0003    CARBON                     SS316LN
MATERIAL         78.               21.45                              PLATINUM
MATERIAL                           21.78                              Ir192
COMPOUND        -0.3   IRIDIUM      -0.7  PLATINUM                     Ir192
MATERIAL                        .00120484                             AIR
COMPOUND   -1.248E-4    CARBON -0.755267  NITROGEN -0.231781    OXYGENAIR
COMPOUND   -0.012827     ARGON                                        AIR
* 276 Water liquid H2O
* Chemical Formula:  H -- O -- H
MATERIAL                            1.0                                WATER
COMPOUND         2.0  HYDROGEN       1.0    OXYGEN                     WATER
ASSIGNMA    BLCKHOLE  BLACKHOL
ASSIGNMA      VACUUM      VOID
ASSIGNMA       WATER    SPHERE
ASSIGNMA     SS316LN     STEEL
ASSIGNMA       Ir192   IRIDIUM
RADDECAY          2.
DCYSCORE         -1.                           dose      dose          USRBIN
USRBIN           11.      DOSE      -40.        9.       0.0       4.5dose
USRBIN           0.0       0.0      -4.5      300.        1.      300. &
RANDOMIZ          1.       10.
START            1E9
STOP
```

APPENDIX C

```
TITLE
GLOBAL        1000.0       0.0       0.0       0.0       1.0        0.
DEFAULTS                                                              PRECISIO
BEAM                                                                  ISOTOPE
BEAMPOS          0.0       0.0       0.0
BEAMPOS                  0.065                 0.36                   CYLI-VOL
HI-PROPE         77.      192.
GEOBEGIN                                                              COMBNAME
    0    0                    MC-CAD
SPH Sphere     0.00 0.00 0.00 30.
SPH extvoid    0.00 0.00 0.00 1000.00
SPH intvoid    0.00 0.00 0.00 500.00
RCC source     0.00 0.00 -0.17 0.00 0.00 0.36 0.065
END
BLACKHOL     5 +extvoid  -intvoid
VOID         5 +intvoid -Sphere
WATER        5 +Sphere -source
IRIDIUM      5 +source
END
GEOEND
MATERIAL         78.               21.45                              PLATINUM
MATERIAL                           21.78                              Ir192
COMPOUND        -0.3   IRIDIUM      -0.7  PLATINUM                     Ir192
MATERIAL                        .00120484                             AIR
COMPOUND   -1.248E-4    CARBON -0.755267  NITROGEN -0.231781    OXYGENAIR
COMPOUND   -0.012827     ARGON                                        AIR
MATERIAL                             1.0                              WATER
COMPOUND         2.0  HYDROGEN       1.0    OXYGEN                    WATER
MATERIAL         77.               22.42                              IRIDIUM
ASSIGNMA    BLCKHOLE  BLACKHOL
ASSIGNMA      VACUUM      VOID
ASSIGNMA       WATER     WATER
ASSIGNMA       Ir192   IRIDIUM
RADDECAY          2.
DCYSCORE         -1.                            dose      dose          USRBIN
USRBIN           11.      DOSE      -41.        9.       0.0       4.5dose
USRBIN           0.0       0.0      -4.5      300.        1.      300. &
RANDOMIZ          1. 17484654.
START            1E9
STOP
```

APPENDIX D

```
TITLE
MasterWork
GLOBAL         5000.       0.0       0.0       0.0        1.
* Set the defaults for precision simulations
DEFAULTS                                                              PRECISIO
* Define the beam characteristics
BEAM                                                                  ISOTOPE
HI-PROPE         77.      192.
* Define the beam position
BEAMPOS          24.       18.        3.       0.0       0.0
* Define the beam position
BEAMPOS          0.0     0.065               0.35                     CYLI-VOL
GEOBEGIN                                                              COMBNAME
VOXELS           0.0       0.0       0.0                             target
    0    0
* Black body
SPH blkbody    0.0 0.0 0.0 1000.
* Void sphere
SPH void       0.0 0.0 0.0 500.
END
* Black hole
BLKBODY      5 +blkbody -void
* Void around
VOID         5 +void -VOXEL
END
GEOEND
MATERIAL         15.               1.82                               PHOSPHO
MATERIAL         16.               2.07                               SULFUR
MATERIAL         17.           0.003214                               CHLORINE
MATERIAL         19.              0.862                               POTASSIU
MATERIAL         30.              7.133                               ZINC
* Skin (ICRU)
*
MATERIAL                           1.1                                 SKIN
COMPOUND   -0.100588  HYDROGEN  -0.22825    CARBON  -0.04642  NITROGENSKIN
COMPOUND   -0.619002    OXYGEN    -7E-05    SODIUM    -6E-05  MAGNESIUSKIN
COMPOUND    -0.00033   PHOSPHO  -0.00159    SULFUR  -0.00267  CHLORINESKIN
COMPOUND    -0.00085  POTASSIU  -0.00015   CALCIUM    -1E-05      IRONSKIN
COMPOUND      -1E-05      ZINC                                        SKIN
* Muscle skeletal (ICRU)
*
MATERIAL                           1.04                                SKELMUSC
COMPOUND   -0.100637  HYDROGEN  -0.10783    CARBON  -0.02768  NITROGENSKELMUSC
COMPOUND   -0.754773    OXYGEN  -0.00075    SODIUM  -0.00019  MAGNESIUSKELMUSC
COMPOUND     -0.0018   PHOSPHO  -0.00241    SULFUR  -0.00079  CHLORINESKELMUSC
COMPOUND    -0.00302  POTASSIU    -3E-05   CALCIUM    -4E-05      IRONSKELMUSC
COMPOUND      -5E-05      ZINC                                        SKELMUSC
* 120 Bone, Compact (ICRU)
*
MATERIAL                           1.85                                Bone_Com
COMPOUND   -0.047234  HYDROGEN  -0.14433    CARBON  -0.04199  NITROGENBone_Com
COMPOUND   -0.446096    OXYGEN   -0.0022  MAGNESIU  -0.10497   PHOSPHOBone_Com
COMPOUND    -0.00315    SULFUR  -0.20993   CALCIUM                    Bone_Com
* 103 Adipose Tissue (ICRU)
* from: ICRU Report #37, 1984, pub. by ICRU, Bethesda, Md, 20814, USA.
MATERIAL                           0.92                                Adipose_
COMPOUND   -0.119477  HYDROGEN  -0.63724    CARBON  -0.00797  NITROGENAdipose_
```

```
COMPOUND   -0.232333    OXYGEN   -0.0005    SODIUM    -2E-05  MAGNESIUAdipose_
COMPOUND    -0.00016   PHOSPHO  -0.00119  CHLORINE                   Adipose_
* Tissue soft (ICRU)
*
MATERIAL                             1.0                              TISSUEIC
COMPOUND   -0.104472  HYDROGEN  -0.23219    CARBON  -0.02488  NITROGENTISSUEIC
COMPOUND   -0.630238    OXYGEN  -0.00113    SODIUM  -0.00013  MAGNESIUTISSUEIC
COMPOUND    -0.00133   PHOSPHO  -0.00199    SULFUR  -0.00134  CHLORINETISSUEIC
COMPOUND    -0.00199  POTASSIU  -0.00023   CALCIUM    -5E-05      IRONTISSUEIC
COMPOUND      -3E-05      ZINC                                   TISSUEIC
* Blood (ICRU)
*
MATERIAL                             1.06                             BLOOD
COMPOUND   -0.101866  HYDROGEN  -0.10002    CARBON  -0.02964  NITROGENBLOOD
COMPOUND   -0.759414    OXYGEN  -0.00185    SODIUM    -4E-05  MAGNESIUBLOOD
COMPOUND      -3E-05   SILICON  -0.00035   PHOSPHO  -0.00185    SULFURBLOOD
COMPOUND    -0.00278  CHLORINE  -0.00163  POTASSIU    -6E-05   CALCIUMBLOOD
COMPOUND    -0.00046      IRON    -1E-05      ZINC                   BLOOD
* Brain (ICRU)
*
MATERIAL                             1.03                             BRAIN
COMPOUND   -0.110667  HYDROGEN  -0.12542    CARBON  -0.01328  NITROGENBRAIN
COMPOUND   -0.737723    OXYGEN  -0.00184    SODIUM  -0.00015  MAGNESIUBRAIN
COMPOUND    -0.00354   PHOSPHO  -0.00177    SULFUR  -0.00236  CHLORINEBRAIN
COMPOUND     -0.0031  POTASSIU    -9E-05   CALCIUM    -5E-05      IRONBRAIN
COMPOUND      -1E-05      ZINC                                   BRAIN
* Skeleton-Red Marrow
* from: Woodward & White, Brit. J. Radiology, vol. 59, 1216 (1986).
MATERIAL                             1.03                             SkeleM
COMPOUND       -10.5  HYDROGEN     -41.1    CARBON      -3.4  NITROGENSkeleM
COMPOUND       -43.9    OXYGEN      -0.2    SULFUR      -0.2  CHLORINESkeleM
COMPOUND        -0.2  POTASSIU      -0.1      IRON                   SkeleM
* Skeleton-Cartilage
* from: Woodward & White, Brit. J. Radiology, vol. 59, 1216 (1986).
MATERIAL                              1.1                             Skeleton
COMPOUND        -9.6  HYDROGEN      -9.9    CARBON      -2.2  NITROGENSkeleton
COMPOUND       -74.4    OXYGEN      -0.5    SODIUM      -2.2   PHOSPHOSkeleton
COMPOUND        -0.9    SULFUR      -0.3  CHLORINE                   Skeleton
* Eye lens (ICRU)
*
MATERIAL                              1.1                             EYE-LENS
COMPOUND   -0.099269  HYDROGEN  -0.19371    CARBON  -0.05327  NITROGENEYE-LENS
COMPOUND   -0.653751    OXYGEN                                   EYE-LENS
* ..+....1....+....2....+....3....+....4....+....5....+....6....+....7..
ASSIGNMA    BLCKHOLE   BLKBODY
ASSIGNMA      VACUUM      VOID
* Voxel cage
ASSIGNMA      VACUUM     VOXEL
* Air
ASSIGNMA         AIR  VOXEL001
* Skin
ASSIGNMA        SKIN  VOXEL002
* Skeletal muscle
ASSIGNMA    SKELMUSC  VOXEL003
* Jaw bone
ASSIGNMA    Bone_Com  VOXEL004
* Fat
ASSIGNMA    Adipose_  VOXEL005
* Pharynx
ASSIGNMA    TISSUEIC  VOXEL006
```

```
* Blood
ASSIGNMA       BLOOD  VOXEL007
* Bone morrow
ASSIGNMA      SkeleM  VOXEL008
* Spine
ASSIGNMA    Bone_Com  VOXEL009
* Spinal cord
ASSIGNMA       BRAIN  VOXEL010
* Tongue
ASSIGNMA    TISSUEIC  VOXEL011
* Teeth
ASSIGNMA    Bone_Com  VOXEL012
* Spinal canal
ASSIGNMA       WATER  VOXEL013
* Dens of axis
ASSIGNMA    Bone_Com  VOXEL014
* Hard palate
ASSIGNMA    Bone_Com  VOXEL015
* Skull
ASSIGNMA    Bone_Com  VOXEL016
* Sinuses/mouth cavity
ASSIGNMA         AIR  VOXEL017
* Brain
ASSIGNMA       BRAIN  VOXEL018
* Medulla oblangata
ASSIGNMA       BRAIN  VOXEL019
* Cerebellum
ASSIGNMA       BRAIN  VOXEL020
* Cartilage
ASSIGNMA    Skeleton  VOXEL021
* Pons
ASSIGNMA       BRAIN  VOXEL022
* Eye
ASSIGNMA    TISSUEIC  VOXEL023
* Lens
ASSIGNMA    EYE-LENS  VOXEL024
* Optic nerve
ASSIGNMA       BRAIN  VOXEL025
* Cerebral falx
ASSIGNMA       BRAIN  VOXEL026
RADDECAY          2.
DCYSCORE         -1.                          Dose   voxel26          USRBIN
USRBIN           10.      DOSE      -49.       40.       40.       20.Dose
USRBIN           0.0       0.0       0.0      400.      400.      200. &
USRBIN           10.      DOSE      -50.       50.       50.       20.Dose1
USRBIN           0.0       0.0       0.0      300.      300.      200. &
USRBIN           12.      DOSE      -22.  VOXEL002                  voxel2
USRBIN      VOXEL002                             1.                   &
USRBIN           12.      DOSE      -23.  VOXEL003                  voxel3
USRBIN      VOXEL003                             1.                   &
USRBIN           12.      DOSE      -24.  VOXEL004                  voxel4
USRBIN      VOXEL004                             1.                   &
USRBIN           12.      DOSE      -25.  VOXEL005                  voxel5
USRBIN      VOXEL005                             1.                   &
USRBIN           12.      DOSE      -26.  VOXEL006                  voxel6
USRBIN      VOXEL006                             1.                   &
USRBIN           12.      DOSE      -27.  VOXEL007                  voxel7
USRBIN      VOXEL007                             1.                   &
USRBIN           12.      DOSE      -28.  VOXEL008                  voxel8
USRBIN      VOXEL008                             1.                   &
```

```
USRBIN          12.      DOSE      -29.  VOXEL009                  voxel9
USRBIN      VOXEL009                          1.                    &
USRBIN          12.      DOSE      -30.  VOXEL010                  voxel10
USRBIN      VOXEL010                          1.                    &
USRBIN          12.      DOSE      -31.  VOXEL011                  voxel11
USRBIN      VOXEL011                          1.                    &
USRBIN          12.      DOSE      -32.  VOXEL012                  voxel12
USRBIN      VOXEL012                          1.                    &
USRBIN          12.      DOSE      -33.  VOXEL013                  voxel13
USRBIN      VOXEL013                          1.                    &
USRBIN          12.      DOSE      -34.  VOXEL014                  voxel14
USRBIN      VOXEL014                          1.                    &
USRBIN          12.      DOSE      -35.  VOXEL015                  voxel15
USRBIN      VOXEL015                          1.                    &
USRBIN          12.      DOSE      -36.  VOXEL016                  voxel16
USRBIN      VOXEL016                          1.                    &
USRBIN          12.      DOSE      -37.  VOXEL017                  voxel17
USRBIN      VOXEL017                          1.                    &
USRBIN          12.      DOSE      -38.  VOXEL018                  voxel18
USRBIN      VOXEL018                          1.                    &
USRBIN          12.      DOSE      -39.  VOXEL019                  voxel19
USRBIN      VOXEL019                          1.                    &
USRBIN          12.      DOSE      -40.  VOXEL020                  voxel20
USRBIN      VOXEL020                          1.                    &
USRBIN          12.      DOSE      -41.  VOXEL021                  voxel21
USRBIN      VOXEL021                          1.                    &
USRBIN          12.      DOSE      -42.  VOXEL022                  voxel22
USRBIN      VOXEL022                          1.                    &
USRBIN          12.      DOSE      -43.  VOXEL023                  voxel23
USRBIN      VOXEL023                          1.                    &
USRBIN          12.      DOSE      -44.  VOXEL024                  voxel24
USRBIN      VOXEL024                          1.                    &
USRBIN          12.      DOSE      -45.  VOXEL002                  voxel25
USRBIN      VOXEL025                          1.                    &
USRBIN          12.      DOSE      -46.  VOXEL026                  voxel26
USRBIN      VOXEL026                          1.                    &
RANDOMIZ         1.324534635.
* Set the number of primary histories to be simulated in the run
START           1E8
STOP
```